SYNTHESIS AND CHARACTERIZATION OF $LiFePO_4$ AND IT'S NANO COMPOSITE FOR SUPERCAPACITOR APPLICATION

Dissertation submitted to

Visvesvaraya National Institute of Technology, Nagpur

In partial fulfillment of the requirements for the award of

the degree

Master of Science

in

Physics

by

Arjun K S

(MS23PHY014)

Under the guidance of

Dr. Sushama M Giripunje

Department of Physics

Visvesvaraya National Institute of Technology

Nagpur 440 010 (India)

May-2025

SYNTHESIS AND CHARACTERIZATION OF $LiFePO_4$ AND IT'S NANO COMPOSITE FOR SUPERCAPACITOR APPLICATION

Dissertation submitted to

Visvesvaraya National Institute of Technology, Nagpur

In partial fulfillment of the requirements for the award of

the degree

Master of Science

in

Physics

by

Arjun K S

(MS23PHY014)

Under the guidance of

Dr. Sushama M Giripunje

Department of Physics

Visvesvaraya National Institute of Technology

Nagpur 440 010 (India)

May-2025

© Visvesvaraya National Institute of Technology (VNIT) 2025

Department of Physics

Visvesvaraya National Institute of Technology, Nagpur

Declaration

I, Arjun K S, hereby declare that this dissertation titled **"SYNTHESIS AND CHARACTERIZATION OF $LiFePO_4$ AND IT'S NANO COMPOSITE FOR SUPERCAPACITOR APPLICATION"** was carried out by me in the Department of Physics of Visvesvaraya National Institute of Technology, Nagpur. The work is original and has not been submitted earlier, whole or in part, for the award of any degree/diploma at this or any other Institution / University.

Arjun K S

(MS23PHY014)

Date:

Certificate

This is to certify that the dissertation titled **"SYNTHESIS AND CHARACTERIZATION OF $LiFePO_4$ AND IT'S NANO COMPOSITE FOR SUPERCAPACITOR APPLICATION"** is submitted by **Arjun K S** in partial fulfillment of the requirements for the award of the degree of **Master of Science in Physics**, VNIT Nagpur. The work is comprehensive, complete, and fit for final evaluation.

Dr. Sushama M Giripunje

Associate Professor

Department of Physics,

VNIT, Nagpur

Head, Department of Physics

VNIT, Nagpur

Date:

Department of Physics

Visvesvaraya National Institute of Technology, Nagpur

Non-Plagiarism Certificate

Certified that M.Sc. Dissertation titled "**SYNTHESIS AND CHARACTERIZATION OF $LiFePO_4$ AND IT'S NANO COMPOSITE FOR SUPERCAPACITOR APPLICATION**" submitted by **Arjun K S**, Enrollment No. **MS23PHY014**, ID No. **30490,** has been checked for plagiarism using TURNITIN software, and an overlap is found within prescribed limits (<30%). A summary of the report is given below:

Arjun K S
(MS23PHY014)
ID No. 30490

Dr. Sushama M Giripunje,
Associate Professor
Department of Physics
VNIT, Nagpur

Acknowledgements

I would like to express my heartfelt gratitude to my guide, **Dr. Sushama M Giripunje,** Associate Professor, Department of Physics, Visvesvaraya National Institute of Technology, Nagpur, for giving me the opportunity and guidance to carry out my M.Sc. project under her. It had given me a wonderful learning experience, and I gained much more insight into the field of nanomaterials and supercapacitor development. She was very supportive and encouraged me to explore the area of nanoscience and to complete my project work effectively.

I would like to thank **Dr. Babasaheb R. Sankapal**, Head of the Department of Physics, VNIT, and **Dr. Premlal Patel**, Director of VNIT, for providing me with the necessary facilities for the completion of my project work.

I am very grateful to **Mr. Diganta Kuar**, Research Scholar, Department of Physics, VNIT, for his support and for giving me new ideas throughout the duration, which were necessary for my project. His valuable advice and knowledge have helped me a lot throughout my project.

I would like to thank all my friends for their valuable support and suggestions.

From the bottom of my heart, I am extremely heartful to my parents and family members, who supported me in all ups and downs, without them, the completion of my project would not have been possible.

Arjun K S

ABSTRACT

Supercapacitors are reliable candidates for the best electrical energy storage devices, and their widespread use has increased the demand for inexpensive, environmentally friendly energy storage solutions. Two-dimensional LFP has excellent thermal stability and is non-toxic, making it safer and more environmentally friendly than many other electrode materials. Even though it is a battery-type material, it can show capacitive behavior when compounded with conductive materials like graphene, CNTs, etc. In this work, lithium iron phosphate/MWCNT was prepared, which is used as an electrode material for supercapacitor application. The addition of MWCNT as a composite material in LFP enhances the electrical conductivity. The structural features were evaluated by XRD, Raman spectrum, and SEM. The performance in various electrolytes was compared through electrochemical analysis conducted in 3M solutions of LiOH, NaOH, and KOH. In 3M KOH, better results were obtained. At a current density of 2A/g, we obtained a specific capacitance of 965.40 F/g and a high-power density of 521.91 W/Kg. The material exhibits capacitance retention of 68.64% over 2000 cycles.

LIST OF FIGURES

Figure No.	Title	Page No.
1.1	Conventional capacitor	3
1.2	Ragone plot	4
1.3	Classification of supercapacitor	5
1.4	Model for electrical double layer: (a) The Helmholtz model, (b) The Gouy-Chapman model, (c) The Stern model.	7
2.1	Structure of $LiFePO_4$	21
3.1	Hydrothermal set-up	23
3.2	(a) solution, (b) Magnetic stirring for 6 hrs, (c) Solution put in autoclave, (d) Hydrothermal setup, (e) Power of LFP after grinding	27
3.3	Initial drying process of the deposited electrode	28
3.4	Schematic circuit diagram for a three-electrode potentiostat system	32
4.1	Diffraction pattern of $LiFePO_4$	34
4.2	Diffraction pattern of $LiFePO_4$ and LiFePO4/MWCNT composite	35
4.3	Comparison between the diffraction peaks of LiFePO4 and LiFePO4/MWCNT composite	36
4.4	SEM images of $LiFePO_4$	37
4.5	SEM images of $LiFePO_4$/MWCNT	37
4.6	Raman spectrum of $LiFePO_4$	38
4.7	Raman spectrum of $LiFePO_4$/MWCNT	39
4.8	EDS Spectrum of $LiFePO_4$	39
4.9	EDS Spectrum of $LiFePO_4$/MWCNT	40

4.10	CV curve of LiOH with different scan rates	41
4.11	CV curve in different electrolytes with a scan rate of 5mV/s	42
4.12	GCD profile at different current densities	44
4.13	Nyquist plot of LFP/MWCNT	45
4.14	Cycling Stability of LFP/MWCNT electrode	46

LIST OF TABLES

Table No.	Title	Page No.
2.1	Comparison between different synthesis methods of LiFePO	20
4.1	Atomic weight% % and weight% of elements in $LiFePO_4$	40
4.2	Atomic weight% % and weight% of elements in LiFePO4/MWCNT	40
4.3	Specific capacitance of LiOH at different scan rates	42
4.4	Specific capacitance of different electrolytes with a scan rate of 5mV/s	43
4.5	The specific capacitance, energy density, and Power density of the electrode for different current densities	44

LIST OF ABBREVIATIONS

Abbreviation	Full form
SC	Supercapacitor
EDLC	Electrochemical Double Layer Capacitor
PC	Pseudo Capacitor
AC	Activated Carbon
SSA	Specific Surface Area
NaOH	Sodium Hydroxide
KOH	Potassium Hydroxide
CNT	Carbon Nanotube
GN	Graphene Nanosheets
$ZnCl_2$	Zinc Chloride
NiO	Nickel Oxide
MnO_2	Manganese Dioxide
V_2O_5	Vanadium Pentoxide
RuO_2	Ruthenium Oxide
HSC	Hybrid Supercapacitor
TMP	Transition Metal Phosphide/Phosphate
TMO	Transition Metal Oxide
CP	Conducting Polymer
PANI	Polyacrylonitrile
PThy	Polythiophene

Ppy	Polypyrrole
SWCNT	Single-Walled Carbon Nanotube
MWCNT	Multi-Walled Carbon Nanotube
rGO	Reduced Graphene Oxide
H_3PO_4	Orthophosphoric Acid
$FeSO_4 \cdot 7H_2O$	Iron (II) sulphate
LiOH	Lithium hydroxide
NMP	N-methyl-2-Pyrrolidone
PVDF	Poly vinylidene fluoride
XRD	X-Ray Diffraction
SEM	Scanning Electron Microscopy
EDS	Energy-Dispersive X-ray Spectroscopy
CV	Cyclic Voltammetry
GCD	Galvanostatic Charge Discharge

LIST OF SYMBOLS

Symbol	Meaning
C	Capacitance
V	Voltage
Q	Charge stored
ε_0	Permittivity of free space
ε_r	Dielectric constant
A	Electrode area
r	Separation between electrode
P_{max}	Maximum power
ESR	Equivalent series resistance
C_{dl}	Capacitance of EDLC
C_H	Stern layer capacitance
C_{diff}	Diffusion region capacitance
n	Order
λ	Wavelength of source
θ	Angle of diffraction
d	Interplanar distance
I	Current
ΔV	Potential window
Δt	Discharge time
w	Mass of the electrode
ϑ	Scan rate
C_s	Specific capacitance
E	Energy density
P	Power density

TABLE OF CONTENTS

ABSTRACT i

LIST OF FIGURES ii

LIST OF TABLES iv

LIST OF ABBREVIATIONS v

LIST OF SYMBOLS vii

CHAPTER 1: INTRODUCTION 1

1.1 Background of supercapacitor 1

1.2 Comparison with conventional capacitor 2

1.3 Application of supercapacitor 4

1.4 Classification of supercapacitor 5

1.4.1 Electrochemical Double Layer Capacitor (EDLC) 5

1.4.2 Pseudo capacitor 7

1.4.3 Hybrid capacitor 8

1.4.3.1 Asymmetric hybrids 8

1.4.3.2 Composite hybrids 8

1.4.3.3 Battery hybrids 9

1.5 Electrode materials for supercapacitor 9

1.5.1 Carbon materials 9

1.5.1.1 Activated carbons (ACs) 9

1.5.1.2 Carbon nanotubes (CNTs) 10

1.5.1.3 Graphene 11

1.5.2 Metal oxide 11

1.5.3 Metal chalcogenides 12

1.5.4 Metal phosphides/ phosphates 13

1.5.5 Conducting polymers 14

1.5.5.1 polyaniline (PANI) 15

1.5.5.2 Polypyrrole (Ppy) 15

1.5.6 Composites 16
1.5.6.1 Binary composites 16
1.5.6.1.1 Carbon-carbon composites 16
1.5.6.1.2 Carbon-MO composite 16
1.5.6.1.3 Carbon-CP composite 17
1.5.6.2 Ternary composites 18
CHAPTER 2: LITERATURE REVIEW 19
CHAPTER 3: EXPERIMENTAL 23
3.1 Hydrothermal 23
3.1.1 Factors affecting the hydrothermal method 24
3.1.1.1 Temperature 24
3.1.1.2 Pressure 24
3.1.1.3 Time 25
3.1.1.4 pH of the solution 25
3.1.1.5 Type and concentration of precursors 25
3.2 Materials used 26
3.3 Synthesis of $LiFePO_4$ 26
3.4 Electrode preparation 27
3.5 Characterization techniques 28
3.5.1 Structural characterization 28
3.5.1.1 X-ray Diffraction (XRD) 28
3.5.1.2 Scanning Electron Microscopy (SEM) 29
3.5.1.3 Raman spectroscopy 30
3.5.1.4 Energy -Dispersive X-ray Spectroscopy (EDS) 31
3.5.2 Electrochemical characterization 31
3.5.2.1 Cyclic Voltammetry (CV) 32
3.5.2.2 Galvanostatic Charge Discharge (GCD) 33
CHAPTER 4: RESULTS AND DISCUSSIONS 34
4.1 Structural characterization 34
4.1.1 X-ray Diffraction (XRD) 34
4.1.2 Scanning Electron Microscopy (SEM) 36

4.1.3 Raman Spectroscopy 38
4.1.4 Energy-Dispersive X-ray Spectroscopy (EDS) 39
4.2 Electrochemical Characterization 41
4.2.1 Cyclic Voltammetry (CV) 41
4.2.2 Galvanostatic Charge Discharge (GCD) 43
4.2.3 Electrochemical Impedance Spectroscopy (EIS) 45
4.2.4 Cycling Stability 46
CHAPTER 5: CONCLUSION 47
REFERENCES 48

CHAPTER 1: INTRODUCTION

1.1 Background of supercapacitor

Due to increasing population growth and technological advancements, the modern world is in a serious shortage of advanced energy sources. The two major categories of energy sources are non-renewable and renewable. Since the beginning of the Industrial Revolution, the nation's social and economic well-being has been highly dependent on the extensive usage of fossil fuels like coal, gas, and oil, which involve non-renewable energy sources. These resources are easily accessible carbon sources. According to calculations, the world's energy consumption from fossil fuels was estimated to be 13.731 billion tons of oil equivalent (BTOE) in 2012, and by 2035, that number will have increased to 18.30 BTOE [1]. However, the use of renewable energy is the primary focus of recent energy technology developments, which will be a better way to address the field's present problems, such as the running out of fossil fuels, rising pollution, and global warming. [2].

Energy sources categorized as renewable are those that have an infinite supply of energy. Examples include solar, wind, biomass, geothermal, and so on. Improving the economy and dependability of the energy supply, taking into account the problems with local water and energy supplies, raising the standard of living and employment of the local population, ensuring sustainable development, and addressing other serious problems will be made possible by the development of renewable energy systems [3]. As using renewable energy sources simply results in reduced pollution, devices that store this energy can be utilized extensively and offer great efficiency, extended lifespans, and reusability. In the context of sustainable development, the development of high-efficiency renewable energy devices is therefore fundamental [4].

A worldwide power supply is required for many applications, and efficient storage of electrical energy from renewable energy sources is required to meet this demand. Dependable candidates for the best electrical energy storage devices are supercapacitors, and their widespread applications have highlighted the demand for a low-cost solution for storing green energy [5]. Supercapacitors (SCs) have generated a lot of attention as a means of connecting

the gap between fuel cells and batteries, which have a high energy density, and conventional capacitors, which have a high power density. Improved energy and power density, almost maintenance-free operation, no memory effect, safety, fast charge/discharge times, and affordability are some of its benefits [6].

1.2 Comparison with conventional capacitor

The three family types of capacitors are supercapacitors, electrolytic capacitors with moist separators, and electrostatic capacitors with dry separators. Electrostatic capacitors are used to tune radio frequencies and filter signals since they exhibit very low capacitance. Even though the capacitance of an electrolytic capacitor is a few microfarads, its size ranges from a few picofarads to low microfarads. It is employed in power coupling, buffering, and filtering. In addition, their storage capacity is a thousand times greater than that of an electrostatic capacitor. The capacitance of a supercapacitor is higher than that of a parallel plate capacitor. [7].

A dielectric material is placed between two conducting plates to create a parallel plate capacitor. When a voltage is applied to the capacitor, the opposite charges will accumulate on the surface of each electrode. Furthermore, an electric field produced by the dielectric that separates the charges allows energy to be stored in the capacitor. [8]. The equation connects a capacitor's capacitance to the charge it holds and the voltage it receives.

$$C=Q/V \tag{1.1}$$

Also, the capacitance (C) is proportional to electrode area (A) and inversely proportional to the distance between the electrodes (r) and is related by the equation,

$$C = \varepsilon_0 \varepsilon_r A / r \tag{1.2}$$

The two major quantities when we consider the working of the capacitor are energy density and power density. The Energy stored in the capacitor is related to capacitance by the equation,

$$E = \frac{1}{2} C V^2 \tag{1.3}$$

The resistance of the capacitance depends on internal parts, such as the electrode
we are using, the dielectric material, and the current collectors. The "equivalent series

resistance" (ESR), which is the combined value of these resistances, is the result. The discharge voltage is determined by these resistances. A capacitor's maximum power, P_{max} is established by

$$P_{max} = \frac{V^2}{4 \times ESR} \tag{1.4}$$

This relationship suggests how ESR can regulate a capacitor's maximum power.

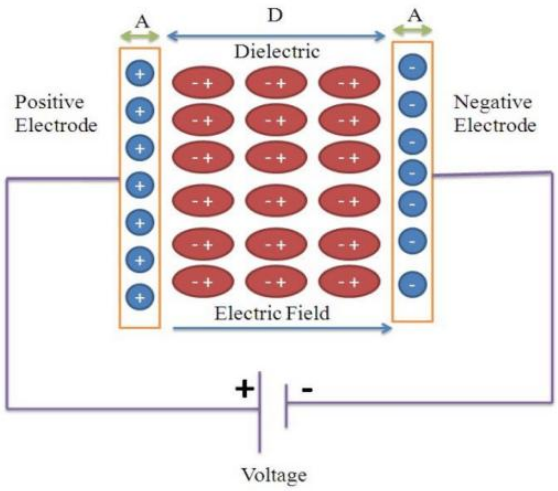

Figure 1.1 Conventional capacitor

Traditional capacitors have relatively higher power densities but lower energy densities than fuel cells and electrochemical batteries. Batteries have a higher total energy storage capacity compared to capacitors, but their power density is lower due to their slow rate of energy release. Because they can quickly release their stored electrical energy to produce a large amount of power, capacitors have a high power density, although they can hold a relatively smaller amount of energy per volume or unit mass. An electrolyte, two electrodes, and a separator that electrically isolates the two electrodes constitute a supercapacitor (SC).

SCs and conventional capacitors operate according to the basic principles. However, these devices are using high surface area electrodes, which give them a higher energy density than capacitors, and thin dielectrics, which reduce the distances between electrodes. They also have many advantages over electrochemical batteries and fuel cells, such as high-power densities, longer cycle and shelf lives, and fast charging times. [8].

By fixing the gap between traditional capacitors and batteries, the Ragone plot (a graphical representation that is used mainly to compare the energy density and power density of these systems), which is displayed in Figure 1.2, illustrates the benefits of SCs by plotting the power density and energy density of various energy storage devices.

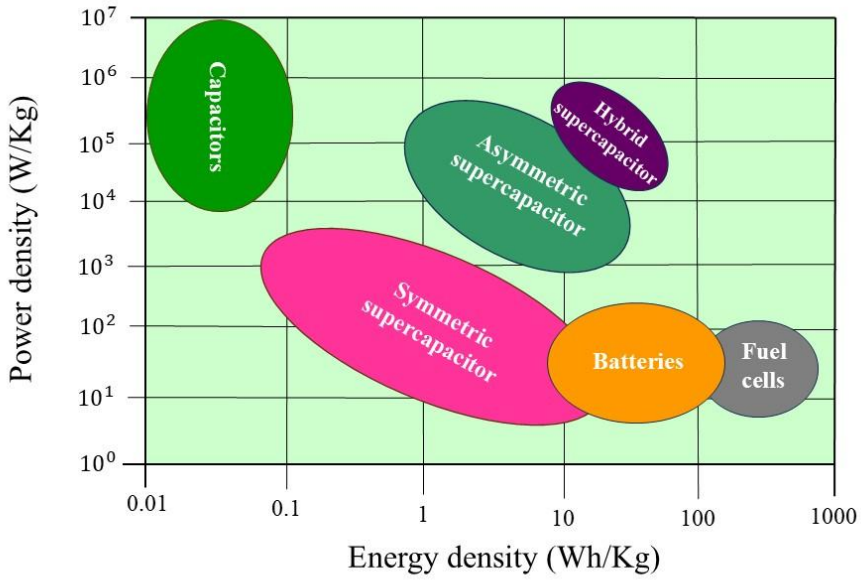

Figure 1.2 Ragone plot

1.3 Application of supercapacitor

SCs are becoming more common and have a promising future in a range of applications for energy storage devices. Because of their many advantages, such as exceptional performance, long lifespan, high specific capacitance, high power density, environmental friendliness, and adjustable operating temperature, SCs are far more significant than other contemporary energy storage technologies. Due to their rapid charging and ability to provide power in a shorter amount of time, they might also be occupying the gaps left by traditional condensers and batteries. These benefits make it ideal for providing electricity in isolated areas without public networks or with costly energy and infrastructure.

Additionally, SCs can be used in a variety of applications, such as the electric grid, rail, electric vehicles, photovoltaic and wind power generation, and more. Because they are

small and versatile, they are commonly used as power supplies for portable electronics such as digital cameras, phones, notebook computers, and so on. Supercapacitors (SCs) can be used in electric and hybrid vehicles to provide the high-power density needed for rapid acceleration and energy recovery during braking, preserving energy and protecting batteries from a rapid high-frequency charge and discharge phase (dynamic operation) [8].

1.4 Classification of supercapacitor

Based on how they are storing charges, the supercapacitors are generally divided into three types. They are shown in fig 1.3

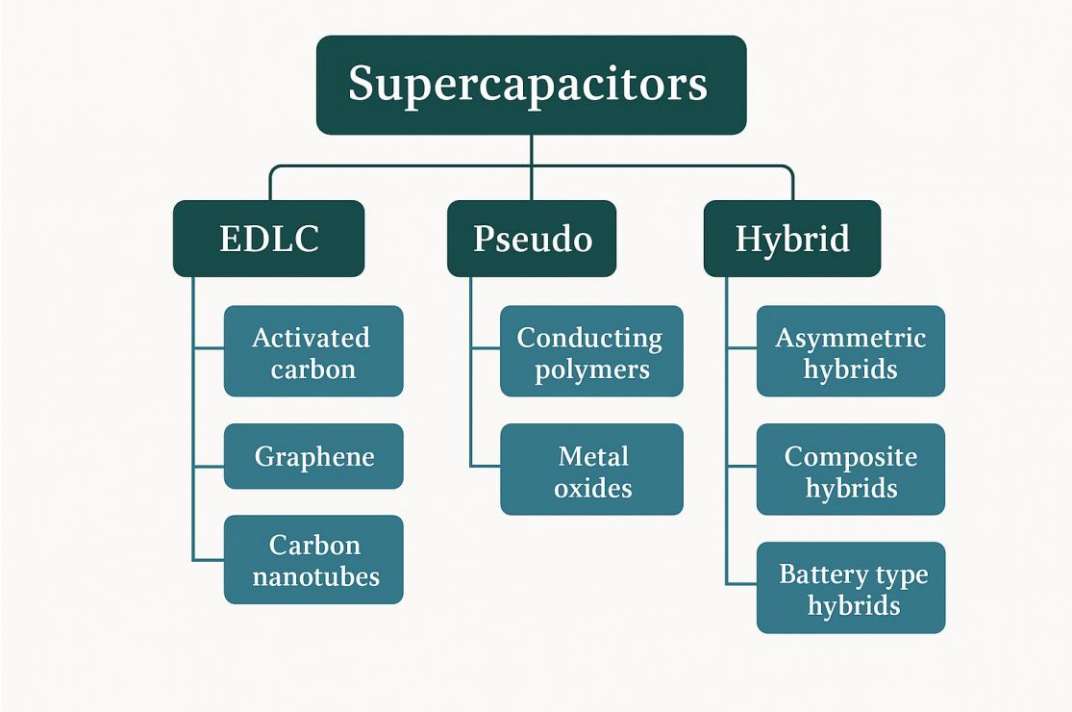

Figure 1.3 Classification of supercapacitor

1.4.1 Electrochemical Double Layer Capacitor (EDLC)

Two carbon-based electrodes, an electrolyte, and a separator compose the EDLC. They store charge electrostatically, or non-Faradaically, instead of transferring it between the electrode and the electrolyte. When voltage is applied, charge accumulates on the electrode

surfaces. Because opposite charges attract, ions in the electrolyte solution pass through the separator and enter the electrode pores with the opposite charge. Double layers, an increase in surface area, and a decrease in the distance between electrodes enable EDLC to achieve higher energy densities than conventional capacitors. Charge storage in an EDLC is highly reversible. Two identical substrate layers are composed of their "virtual" plates. Since the double-layer can handle a low voltage, higher voltages are achieved by matching series-connected individual EDLC [7]. Helmholtz first proposed and developed the idea of EDLCs in the 19th century while studying opposite charges on the surfaces of colloidal particles, as schematically depicted in Fig. 1.4(a). The model that is suggested characterizes opposite charges as being layered at the electrode/electrolyte interface and separated by an atomic distance, much like two-plate conventional capacitors. The diffusive layer model was developed by Gouy and Chapman from the Helmholtz model (fig.1.4(b)). Furthermore, Stern created a hybrid model between the Helmholtz and Gouy-Chapman models to identify two zones of particle distribution: a diffusive layer and an inner region known as the Stern layer (compact layer) (Fig.1.4(c)). Ions function well as an adsorbate for the conductor inside the Stern layer because they are frequently hydrated.

Furthermore, the compact layer contains both particular adsorbate ions, which are frequently anions regardless of the type of electrode charge, and nonspecific adsorbate counter-ions. The two distinct types of adsorbed ions are found in the inner and outer Helmholtz planes. The thickness influences a diffuse double layer formed by the kinetic energy of counter ions, according to the Gouy–Chapman model, which explains the diffusive layer region. The capacitance for an EDLC (C_{dl}) is the sum of the diffusive region capacitance (C_{diff}) and the Stern layer capacitance (CH). The equation can be expressed as follows. [1]

$$\frac{1}{C_{dl}} = \frac{1}{C_H} + \frac{1}{C_{diff}} \tag{1.4}$$

EDLCs employ an electrostatic charge storage method with carbon-based electrodes that are electrochemically inactive, such as graphene, carbon nanotubes (CNTs), activated carbons (ACs), etc. Among the benefits of EDLCs are increased mechanical stability, chemical stability, improved specific surface area, and remarkable electrical conductivity. [9].

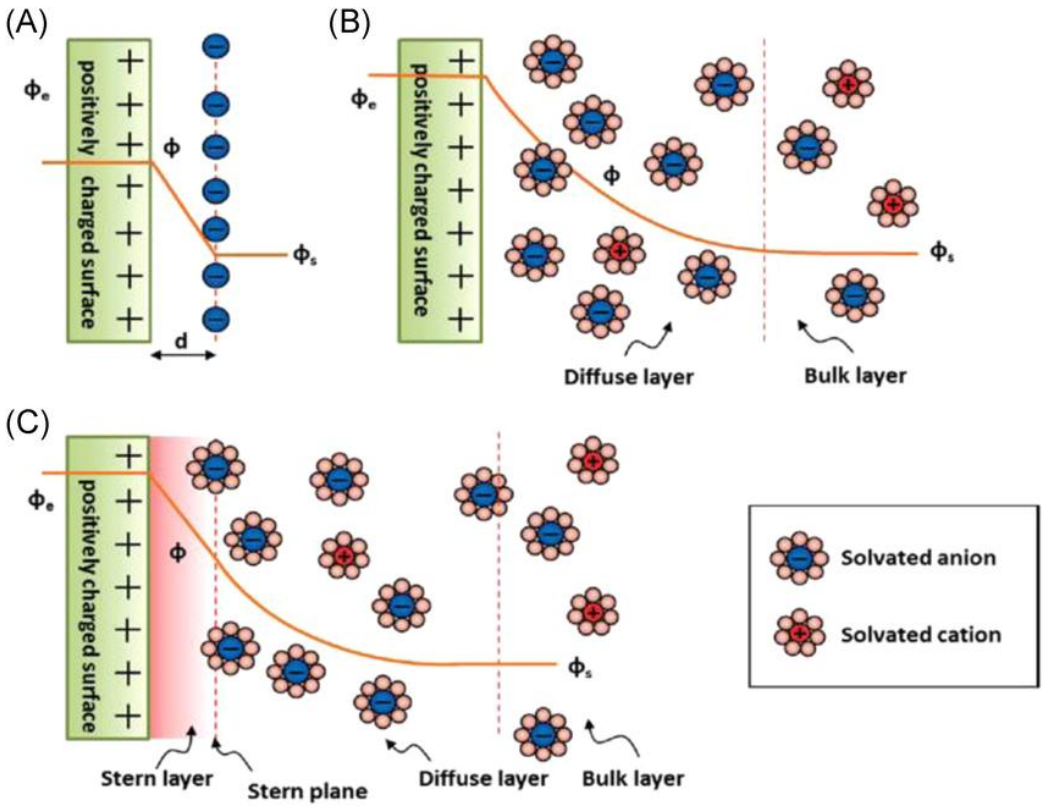

Figure 1.4. Model for electrical double layer:(a) The Helmholtz model,(b) The Gouy-Chapman model, (c) The Stern model.

1.4.2 Pseudo capacitor

It is the kind of supercapacitor with a high electrochemical pseudo-capacitance and electrodes made of conducting polymers or metal oxides. The charge transfer between the electrode and electrolyte is happening due to a Faradaic mechanism, just like in oxidation-reduction reactions. When a potential is applied to the pseudo-capacitor, it causes reduction and oxidation, which involves the passage of charge through a double layer on the electrode material. This is how the faradaic current flows through an SC cell.

In PC devices, the bulk or surface adjacent to the solid electrode surfaces obtains the majority of the electric charge. To demonstrate the voltage-dependent charge transfer process, a faradaic reaction consequently takes place during contact between the electrolyte and the solid material. Because of this, PC is voltage-dependent. PC ultra-capacitors have been invented using three common electrochemical processes: doping/de-doping of CP materials in the electrode, surface adsorption of electrolyte ions, and redox reactions involving

electrolyte ions. Because the first two processes mainly rely on surface mechanisms, their efficiency is highly dependent on the specific area of the electrode materials. Because the final process, which uses CP materials in the electrode, is bulk-based, surface area has less of an impact on capacitance. The electrode materials must always exhibit their maximum level of electronic conductivity to make sure that the electric current is dispersed and collected [1]. Additionally, the Faradic process makes pseudo-capacitors to achieve higher specific capacitance and energy densities than EDLCs.

1.4.3 Hybrid capacitor

The electrodes of this kind of supercapacitor are asymmetrical, with one of them mainly electrostatic and the other electrochemical. Additionally, hybrid capacitors' combined performance offers advantages that were previously impossible to achieve. Additionally, they are combining the advantageous aspects of pseudo-capacitors and EDLCs to create a single SC. Efforts to make better hybrid capacitors and more precise quantitative models of them were still ongoing, despite hybrid capacitors receiving less research attention than pseudo-capacitors or EDLCs. Due in part to their remarkably simple performance and design tuning and the growing emphasis on creating high-energy and high-cycle-life SCs, hybrid capacitors have overtaken EDLCs as the most prevalent class of SCs. Based on the differences in their electrode configurations, there are three types of hybrid capacitors were differentiated: asymmetric, composite, and battery-type.

1.4.3.1 Asymmetric hybrids

Asymmetric hybrid capacitors incorporate faradic and non-faradic processes by attaching an EDLC to a pseudo-capacitor electrode. As a result, the conducting polymer or metal oxide operated as the positive electrode and the carbon material as the negative electrode.

1.4.3.2 Composite hybrids

Composite electrodes consist of carbon-based materials with metal oxides or polymer conduction, showing that the single electrode will have two distinct energy storage processes: chemical and physical. There are two types of composites: ternary composites, which are

made of three different materials, and binary composites, which are made of only two materials.

1.4.3.3 Battery hybrids

An unusual combination of a battery electrode and an SC electrode. This concept demonstrates the need for higher power batteries and high energy capacitors by combining the SC recharging times and battery qualities. It also achieves both battery and SC characteristics in a single cell. There are the least number of studies going on for Battery-type hybrids [8]

1.5 Electrode materials for supercapacitor

Enhancing the performance of SCs involves choosing the appropriate electrode material and fabricating it correctly. SC electrodes must have the following qualities: corrosion resistance, chemical stability, high electrical conductivity, thermal stability, high specific surface area (SSA), and suitable surface contact. They should be affordable and environmentally friendly. More than that, their ability to transfer the faradic charge is essential for enhancing the supercapacitor's performance. The specific capacitance is also affected by several other important variables, including the direct control of morphology, which includes pore size distributions, pore shape, pore diameters, and their electrolyte availability.

Therefore, the two most important criteria for designing an SC device are optimizing the electrochemically active sites by selecting electrode materials with a large SSA and changing the size and shape of the electrode material's pores, which makes it easier to transport electrolyte ions.

1.5.1 Carbon materials

1.5.1.1 Activated carbons (ACs)

Activated carbon is the most widely used substance for EDLC electrodes. Its complex porous structure, which contributes to a high SSA, includes macropores larger than 50 nm, mesopores between 2 and 50 nm, and micropores smaller than 2 nm. It is also reasonably priced. Additionally, they are still suitable for SCs despite having a lower outstanding electrical conductivity (1250–2500 Sm−1).

To generate activated carbon, various carbon-rich organic precursors, including wood, coconut shells, coke, fossil fuels, and synthetic polymers, must be chemically or physically activated. The carbonization stage involves heating precursors to oxidizing gases, including air, steam, and CO2, at high temperatures (700–1200◦c) in an ambient atmosphere to produce amorphous carbon. During the activation process, a lower temperature (between 400°C and 700°C) is applied. The chemical activation process is carried out in the presence of substances like carbonates, alkalis, chlorides, or acids like KOH, $ZnCl_2$, NaOH, etc., to produce a porous network in the bulk of the carbon particles. In addition, because the ion size for the organic electrode is larger, the specific capacitance value for the activated carbon electrode in aqueous electrolyte is higher than in organic solution. The low density of activated carbon is one of its primary drawbacks.

1.5.1.2 Carbon nanotubes (CNTs)

Carbon nanotube electrodes are a useful electrode material due to their unique internal network of mesopores, their accessible outward structure with high SSA, their superior electrical conductivity, low mass densities, and their chemical and thermal durability. In addition, their mechanical flexibility and open network structure allow them to connect to active material, enhance interlinking, and produce a uniform distribution, all of which contribute to the more popular SSA.

CNT electrodes have lower ESR and, therefore, more power than ACs due to the mesoporous structure of CNT networks, which makes it easier and faster for the electrolyte ions to spread. To create a composite that would be utilized as the electrode material for SCs, CNTs may be combined with graphene, metal oxides (MOs), and polymers. They have also described an intriguing phenomenon known as "electro-activation," in which the specific capacitance of graphene and graphene/CNTs is increased and does not decrease after extended cycling in the 1 M KCl electrolyte. The two main forms of carbon nanotubes are SWCNTs and MWCNTs. CNTs can generally be produced by catalytically breaking down certain hydrocarbons. Certain parameters, like crystalline ordering, can be altered to produce different conformations, like SWCNTs and MWCNTs. Electrolyte ions can only access the outermost

surface of SWCNTs due to their tendency to bundle, which decreases their surface area. Low SSA is the limitation on the use of CNT in high-performance SCs.

1.5.1.3 Graphene

Graphene is a two-dimensional, layered substance that is one atom thick and composed of carbon atoms connected by sp^2 bonds arranged in a honeycomb-like crystal structure. Graphene is a remarkable carbon material with remarkable mechanical, morphological, and electrical conductivity, a large surface area, high carrier mobility, and excellent chemical stability. In addition, graphene's two-dimensional structure makes for a thinner electrode, which improves flexibility, thermal and chemical stability, and potential window size. Because of these characteristics, graphene is a desirable choice for energy storage applications. Therefore, unlike other carbon-based materials like ACs and CNTs, graphene-based electrodes are independent of the solid-state pore distribution, making graphene a potential electrode material for high-performance SC applications. An additional advantage of employing graphene as an electrode material is the electrolyte's capacity to reach both of the sheets' exterior surfaces.

Considered as graphene paper, graphene nanosheets (GNSs) can be used as an electrode material in 2D or 3D structures. In the case of 2D graphene, the interplanar π-π interactions and van der Waals forces between the graphene sheets may result in layer stacking, which decreases the SSA and restricts ion diffusion from the electrolyte, thereby lowering electrochemical performance [10].

1.5.2 Metal oxide

Co_3O_4, NiO, RuO_2, $MnO_2$and V_2O_5 are the primary transition metal oxides under the pseudo-capacitor electrodes. Capacitance increases when these metal oxides transition between multiple oxidation states at specific potentials. Ruthenium oxide (RuO_2) is a highly significant material in both crystalline and amorphous forms, both theoretically and practically, due to its many properties, such as its catalytic activities, metallic conductivity, high chemical and thermal stability, electrochemical oxidation-reduction characteristics, and field-emitting behavior. Ferroelectric films, electronic applications, integrated circuit

development, and thin or thick resistors are just a few of the many uses for RuO_2 due to these characteristics. The most recent use of RuO_2 is in SC electrode materials.

RuO_2's long life cycle, highly reversible oxidation-reduction process, wide potential window, highly specific capacitance, and metallic type conductivity make it the most effective metal oxide to use as an electrode material. About SC applications, RuO_2 has been produced via the electrochemical electrodeposition technique. Additionally, at a scan rate of 5 mV/s, the subsequent electrodes showed a 498 Fg-1 specific capacitance and remained stable for a significant number of cycles. In catalysis, ion exchange, energy storage, biosensors, and molecular adsorption, manganese oxide (MnO_2) is used extensively. MnO_2 has been the focus of numerous investigations due to its distinct chemical and physical characteristics. It was a very important electrode material for solar cells because of its low cost, good capacitive capabilities in aqueous electrolytes, and environmental friendliness. Nickel oxide (NiO) is a valuable electrode material for solar cells because of its cost-effectiveness, ease of synthesis, and environmentally friendly behavior. Among the many advantages of the electrochemical approach are its precision, affordability, adaptability, dependability, and ease of use. By using an electrochemical process, $Ni(OH)_2$ has been transformed into NiO [8]

1.5.3 Metal chalcogenides

Over the past 20 years, the anisotropic nature of metal chalcogenides (MCs) has gained attention for these significant compounds in both science and industry. When elements from groups IV to VII B transition with elements from the VI A group, like S, Se, and Te, layered binary stable crystalline formations are usually created. As an exception, the band gap is nearly zero for pristine graphene, but it varies depending on the number of layers, elemental combination, and atom presence or absence in transition MCs. Most transition MCs share nearly the same structure and properties as semi-metallic pristine graphene. Thus, their bandgap value falls between 0 and 2 eV.

Transition metal chalcogenides (MCs) have garnered significant attention for a variety of applications, including consumer electronics, electric tools, hybrid vehicles, and more, because of their increased stability and life cycle, as well as their superior safety tolerance over batteries. Nevertheless, due to their superior properties, MCs are also commonly utilized

in SCs and have been applied to the fields of memory devices, fuel cells, solar cells, sensors, LEDs, lithium-ion batteries, and electrocatalysts. These include the following: (i) longer lifespan; (ii) providing additional reactive sites; (iv) improving conductivity and reducing inner resistance and ohmic loss; (v) having short electron transport channel lengths; and (vi) displaying quantum-size effects. Metal sulfides, in particular, perform significantly in electrochemistry. This is primarily due to their stronger electrochemical activity, higher electronic conductivity, and enhanced mechanical and thermal resilience. However, it is well known that the size, crystalline phase, composition, structural features, and electrode design of the electroactive material all significantly affect the performance of the electrochemical energy storage device. Because of their rich redox chemistry, enhanced electronic conductivity, and enhanced mechanical and thermal durability, metal selenides, a novel class of battery-like electrode materials, are attracting attention as possible supercapacitor electrode materials.

1.5.4 Metal phosphides/ phosphates

Transition metal phosphides/phosphates (TMPs), which are made of phosphorus and one or more transition metal elements, are the most promising electrode materials for hybrid supercapacitors (HSCs). They are a desirable material for electrode fabrication because of their strong electrochemical activity, good electrical conductivity, and metalloid characteristics. Compared to TMOs, transition metal phosphides have a higher specific capacity and better rate capability. P, which has a larger atomic radius and a lower electronegativity than O, gives phosphides their unique physicochemical characteristics. [11].

The term “phosphate” (PO_4^{3-}) refers to pentavalent phosphorus oxyanions. Because of their many advantages, such as their low cost, abundance, non-toxicity, superior electric conductivity, mechanical and chemical stability, and high theoretical specific capacitance, transition metal phosphates are gaining popularity as an exotic class of electrode material for SCs and other applications. Their outstanding achievements in ion exchange, interface chemistry, material science, etc., drew the attention of the scientific community in 1987 and 1990. TMPs outperform metal hydroxides or oxides in terms of electrical conductivity and versatility when it comes to fine-tuning the nanostructures. Furthermore, in contrast to

conducting polymers like polypyrrole, polyaniline, polythiophene, etc. TMPs have a lot greater stability. TMP nanostructures are highly tunable, like carbon-based materials, which is beneficial for conductivity within and between particles. There has been a lot of interest in certain TMPs. Transition metal oxides, carbon-based materials, and conducting polymers as an unidentified substitute material for the SC electrode material that has been thoroughly studied. The usage of TMPs as pseudocapacitive electrodes has been extensively studied due to their exceptional charge conductivity. [9].

1.5.5 Conducting polymers

Conducting polymers are another kind of pseudocapacitive electrode material that has been thoroughly studied. These materials are inexpensive, easy to make, have a minimal environmental impact, high Ed, enhanced conductivity in doped states, and high voltage windows. Through chemical alteration, they also show good conductivity and a comparatively high capacitance. CPs can store the charge in their bulk because the charge/discharge operation doesn't result in any structural alterations, such as phase transitions. As a result, CPs can provide a higher capacitance due to their larger surface areas and redox storage capabilities. The capacitance, conductivity, and ESR of CPs are smaller than those of other carbon-based electrode materials. The rapid-reversible redox reactions brought on by the π-conjugated polymer chains are the source of the particular capacitances in CPs. The ions move to the polymer's base during the oxidation process and then return to the electrolyte during the reduction process. Regardless of all the advantages, the reduction-oxidation process of CP causes mechanical stress, which restricts stability and limits degradation over numerous charging-discharging cycles. Another disadvantage of CPs that restricts their efficiency is their slow ion diffusion rates in bulk, which result in a decrease in power density.

CP-based SC electrodes can be made in three different configurations: (a) p-p type, in which both electrode materials are p-doped polymers; (b) n-p type SCs, in which both electrode materials are made of the same polymers, but one is negatively charged and the other is positively charged; and (c) p-doped and p-p' SCs with two distinct p-doped CPs with different oxidation and reduction reactions. There is a great deal of promise for higher power and energy densities, especially with the n-p type polymer conformation. The CP electrode

materials have hindered pseudo-capacitors from reaching their full potential due to low cycling stability and a lack of good n-doped conducting material. Several CPs are commonly utilized for SC electrodes, including PANI, Ppy, polythiophene (PTh), polyindole (PIND), poly 3,4 ethylenedioxythiophene (PEDOT), and polyfuran. PANI and PPy can only be p-dopable, and their n-doping potential is much lower than that of the typical electrolyte. In contrast, PTh can be n-doped or p-doped, along with their different derivatives.

1.5.5.1 Polyaniline (PANI)

PANI is one of the most widely used CP electrode materials because of its high conductivity, low mass, superior capacitive performance for energy storage, simplicity in preparation, and affordability. PANI is also mechanically flexible and safe for the environment.

Despite these advantages, PANI's performance may rapidly deteriorate because of its frequent cycles of swelling and shrinking during charging and discharging. PANI and carbon materials were mixed to form a PANI layer to address this problem. To create a ternary hybrid composite (PANI/MOs/carbon), this layer was subsequently applied on top of the MOs/carbon composite. This increased capacitance and provided PANI with greater cycle stability. PANI has a wide range of electrochromic properties, including color changes, due to its multiple oxidation and protonation forms. These characteristics make it a good choice for the production of electrochromic SCs.

1.5.5.2 Polypyrrole (Ppy)

Energy storage devices require high-performance electrode materials, which can be found in structurally controlled hydrogels of conductive polymers with mechanical flexibility and variable characteristics. One example of a conductive polymer that scientists are too busy to investigate is ppy. It has a higher density and is more flexible than other CPs. Ppy has a high electrical conductivity value between 10 and 500 Scm^{-1} and can withstand a fast redox reaction to store charge. For example, a conductive polypyrrole hydrogel nanostructure was produced by an interfacial polymerization technique, yielding a 3D porous PPy network with a high specific capacitance of 380 Fg^{-1}.In another case, the Lignin-PPy composite was made

by coating lignin with PPy. Through this process, PPy was polymerized both with and without methyl orange present, resulting in PPy films with globular and nanotubular morphologies. The experiment is conducted by pyrolyzing carbon-based material composites in nitrogen atoms in a nitrogen environment. Reports state that the SSA of synthetic materials is ten times higher than that of materials composed solely of carbon [10].

1.5.6 Composites

Hybrid supercapacitors are composed of composite materials. By mixing carbon materials with conducting polymers or metal oxides, composite materials combine aspects of both pseudo-capacitor and EDLC materials, such as a faradaic and non-faradaic mechanism. Carbon nanotubes (CNTs) and polypyrrole together produce supercapacitor electrodes with more capacitance than either material alone.

1.5.6.1 Binary composites

1.5.6.1.1 Carbon-carbon composites

The higher capacitance in the carbon material is caused by the total Specific surface area that is available to the electrolyte ions. Consequently, higher power and energy densities in SC are the outcome of raising the specific surface area of carbon-based materials. Many types of carbon materials can be used to create carbon-based composites. Graphene dispersion is challenging and requires improvement. To offer a remedy, non-covalent functionalized graphene was created. The material's tendency to restack and aggregate as a result of van der Waals forces during the reduction mechanism is another drawback of this substance. This makes the surface area less accessible to the electrolyte ions. The restacking difficulty will be solved by employing SWCNTs to supply the intrapore for the solution.

1.5.6.1.2 Carbon-MO composite

By mixing TMOs and carbon, the nanocomposite can improve the SCs' performance. As a result, there are various MO and carbon-based material composites besides simple and mixed MOs; these composites have shown a larger surface area than pure metal oxide and carbon material.

One of CNTs' most important advantages is their capacity to be surface functionalized by a range of substances, such as MOs and CPs, or to be oxidized to alleviate a problem caused by specific contaminants. Evaluating the performance of pure materials with nanocomposite materials is therefore a topic of much research. Different carbon-based materials and their composites have been examined for use in SC electrodes according to several criteria, including specific capacitance, pore size, stability, rate capability, surface area, and cost. In addition to being cheaper and more stable, carbon materials are thought to be the most effective choices for electrode synthesis. They may also provide good performance, high specific capacitance, and good rate capability. MOs are the fundamental blocks of composites.

1.5.6.1.3 Carbon-CP composite

CPs can be combined with different carbonaceous materials to form a nanocomposite. A nanocomposite consisting of activated carbon as the cathode and CPs as the anode, for instance, can provide higher energy and power density compared to EDLCs and better cycling performance than pseudo capacitors. PANI can be used to generate a wide variety of electrode types. Single-phase PANI materials have been extensively investigated as possible SC electrodes, even though their low-rate capability and extremely poor cycle stability restrict their applications. A range of nanocomposites that are better than PANI or carbon-based electrodes can be created by combining PANI nanostructures with carbon-based materials. In these applications, carbon-based materials are important because they can be viewed as an efficient stabilizer for PANI materials, which are widely accessible in a range of morphologies.

For example, the electro-deposition technique was used to coat the reduced graphene oxide (rGO) aerogel with PANI arrays, leading to a composite of rGO aerogel and PANI. The low cyclability, energy density, and flexibility of rGO aerogel generally limit its use. The resulting composite showed a rich open pore network, high capacitance, and high conductivity due to the unique capacitance of the PANI, which was caused by the 3D interconnected framework of aerogel. The resultant composite was said to have a specific capacitance of 432 Fg^{-1} for a current density of 1 Ag^{-1}, and the materials showed remarkable stability under various bending conditions.[10].

1.5.6.2 Ternary composites

Creating synergistic multiple composites is a practical way to improve the capacitance performance and cycle life of supercapacitor electrodes [12]. For instance, F. Usman et al. created a ternary composite made of PANI, reduced graphene oxide (rGO), and chitosan [13]. Significant PANI properties would be added to the chitosan/graphene oxide and chitosan/reduced graphene oxide composites. Additionally, the RGO enhanced the chitosan/PANI composites' conductivity and thermal stability. Graphene's high surface area to volume ratio was also important for optical, electrical, and optoelectronic applications. The best features of rGO, the advantages of PANI, and the intriguing properties of chitosan, such as its exceptional flexibility, biocompatibility, and biodegradability, are thus combined in this ternary composite**.**

Another study by T. Das et al [14] Created a ternary composite system with manganese cobaltite, acetylene black, and polyaniline. An $MnCo_2O_4$ and polyaniline binary system may exhibit superior electrochemical activity. A notable drawback of the polyaniline and MnCo2O4-based system is the abrupt volume change that occurs during charging and discharging. This problem requires the creation of a hybrid system, which might offer more strength and stability than binary and individual systems. Acetylene black, a carbon material, has been used to create a hybrid ternary system that may boost capacitance and offer stability throughout its life cycle. Acetylene black preserves the intrinsic qualities of polyaniline and $MnCo_2O_4$ by supporting their mechanical degradation brought on by redox reactions.

CHAPTER 2: LITERATURE REVIEW

The use of supercapacitors (SCs) is prominent nowadays due to their rapid charging and discharging capabilities, long lifespan, and ability to handle high current loads. This technology is taking the energy storage industry to another level [15]. Considering batteries, they provide high energy density but are very low in terms of power density. Also, they give a long charging duration but fewer charging cycles [16]. Now, in the case of the supercapacitor, it has less energy density but gives a better value of power density and cycle life. But due to its lower power density value, SC applications are constrained [17], [18]. HSCs collaborate with electric-double-capacitors and pseudocapacitive materials and accomplish a balance between energy density and power density. [15]. The arrangement of the hybrid makes it easier for charge and discharge in a few times. This also provides another merit in enhancing the cycle life [19].

Many works have been done to find effective electrode materials that can deliver high energy and power simultaneously, since they are crucial in determining the performance of SC. Lithium-ion capacitors have attained a significant role in the supercapacitor industry in recent years due to their increased energy density without changing their power density. The first lithium-ion capacitors (LICs) were given rise by Amatucci et al. [20] A few examples of the various kinds of lithium-based supercapacitors are lithium titanate (Li_2TiO_3), lithium cobalt oxide ($LiCoO_2$), and lithium manganese oxide ($LiMn_2O_4$). The best alternative to conventional lithium-based electrodes has been determined to be lithium iron phosphate (LFP). The chemical formula for LFP is $LiFePO_4$, and it is a well-known substance in the energy storage device industry because of its remarkable chemical and thermal stability, low toxicity, and extended cycle life. Additionally, because iron is so abundant, manufacturing costs will decrease.[21]

Paulo F. R. Ortega et al. [22] reported that the low cost of the precursor materials, their low toxicity, and their high thermal and chemical stability led to the strategic selection of $LiFePO_4$ as electrode for the hybrid device under investigation, also it is giving better potential range approximate 3.4v compare to the anode limit 5v, this gives a trustable and secure

operation. The theoretical capacity of $LiFePO_4$ is 170 mA h g−1, it comes relatively high. From the paper of M H Ho et al. [23] reported that by adding LFP to the ordinary carbon electrode, the specific capacitance was increased. Initially carbon electrode shows the specific capacitance of 76.24 F/g in a 1M solution of Na_2SO_3. Then 40 wt% of LFP is added, the after testing, they get the maximum capacitance of 112.41 F/g. From this, we are getting an idea about the material we are using in our experiment that can able to store charges. There are different methods for the synthesis of LFP, including microwave treatment, spray thermal decomposition, the sol-gel method, and the hydrothermal method. These techniques can create LFP particles with a homogeneous size distribution and excellent purity, which can enhance electrochemical performance. But each method has both advantages and disadvantages mentioned in Table 2.1.

$LiFePO_4$	**Advantages**	**Disadvantages**
Microwave-assisted synthesis	Pure products, control over reaction parameters, green raw materials (H_20, alcohols)	Expensive equipment for unfeasible reaction monitoring
Spray pyrolysis	Narrow particle size distribution, homogenous preparation	Plethora of parameters to control (solute concentration, temperature, temperature gradient, residence time in furnace, and carrier gases)
Sol-gel	Homogeneous and high-adhesion products, low-temperature processing	Safety matters are concerned since countable amounts of by-products are released in the calcination step, long growth period
Hydrothermal method	Simple, easy, and low-cost method, production of high-quality nanostructures through easy control of growth parameters	Long growth period

Table 2.1 Comparison between different synthesis methods of $LiFePO_4$ [24]

By analyzing Table 2.1, we can see why the hydrothermal approach works better than the others. Using the precursors lithium hydroxide (LiOH), iron sulphate heptahydrate ($FeSO_4$.

$7H_2O$), and phosphoric acid (H_3PO_4), Dimitra Vernardou et al.[24] prepared a solution in deionized water and performed hydrothermal treatment in a range of temperatures using an autoclave, demonstrating that better results are obtained at a temperature of 200 °C.

Lithium-based electrodes are more frequently utilized in supercapacitors; however, the structure of LFP is also crucial. In 1997, a group that included Goodenough first presented LFP. It is a polyanion substance known as olivine that crystallizes in an orthorhombic system with a slightly warped hexagonally densely packed oxygen arrangement [24].

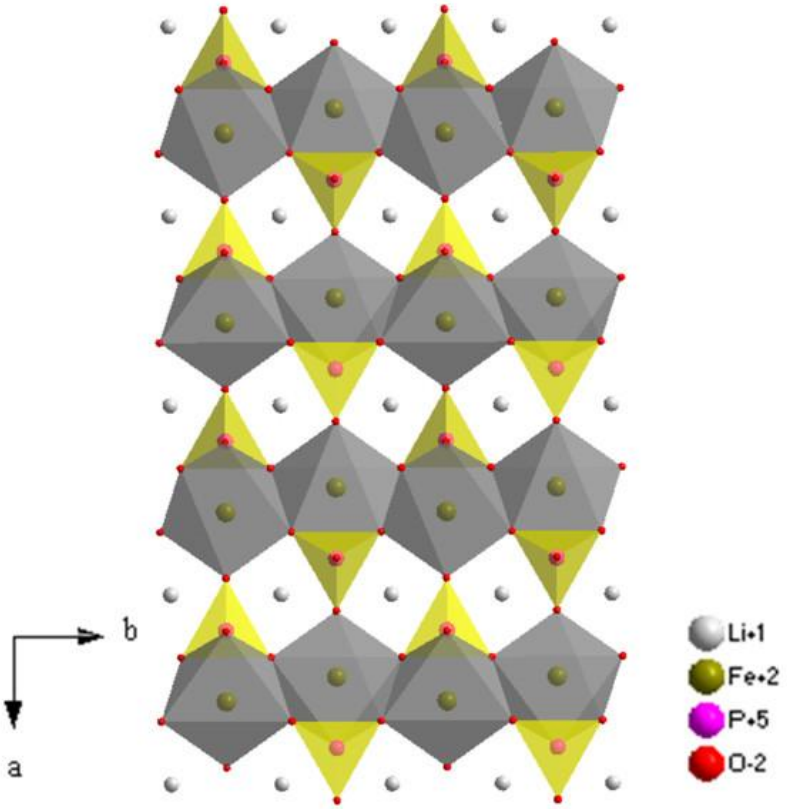

Figure 2.1 Structure of $LiFePO_4$

Figure 2.1 displays the LFP's basic structure. The olivine structure is made up of hexagonally closely packed oxygen atoms, a phosphorus atom in the tetrahedral position, and the remaining iron and lithium atoms occupying the octahedral site. Layers are formed in the b-c plane by the four FeO_6 octahedra that surround each other through shared corners. A 3D network is created by stacking these layers along the axis by sharing two corners and one edge

of the PO_4 tetrahedra. Because of the special structure of LFP, the lithium ions can move back and forth within the crystal lattice. While residing in 1D tunnels [25].

$$LiFePO_4 \underset{\text{charging}}{\overset{\text{Discharging}}{\rightleftharpoons}} FePO_4 + Li^+ + e^-$$

LFP has certain disadvantages in addition to its many advantages. The diffusion coefficient and electrical conductivity are getting close to their lower values, although it has the capacity to store charges. The electrical conductivity of plain LFP is between 10^{-9} and 10^{-11} S/cm, according to N.W.K. Wan et al., while the diffusion coefficient is between 10^{-11} and 10^{-13} S/cm. Another factor impeding the reduction of the electrochemical properties is surface instability [21]. However, adding metals, metal oxides, or carbon materials can help with this issue. Carbon-based materials work better than others at resolving conductivity problems. Composite LFP is made from carbon materials, including graphene, activated carbon, single-walled carbon nanotubes (SWCNTs), and multi-walled carbon nanotubes (MWCNTs). In terms of electrical conductivity, graphene is the most conductible material, followed by MWCNT, SWCNT, and activated carbon.

The primary goal of this work is to create a $LiFePO_4$/MWCNT composite using the hydrothermal method. This composite can enhance electron transport and electrolyte diffusion, making it more appropriate for energy storage applications and providing a useful alternative for the material's use in supercapacitors. The material's properties have been studied through structural and electrochemical characterization.

CHAPTER 3: EXPERIMENTAL

3.1 Hydrothermal

A simple and effective method for producing a range of materials is hydrothermal. It has been found that improving hydrothermal conditions helped to supplement lithium, which in turn improved the electrochemical performance [26]. The process involves conducting chemical reactions in solvents housed in sealed vessels; heating the solvents simultaneously with autogenous pressure allows the solvents' temperature to be raised to approximately critical points. Because water is utilized as a solvent in this process, it is known as "hydrothermal." A sealed stainless-steel autoclave is used to heat an aqueous mixture of precursors above the boiling point of water. The pressure inside the reaction autoclave is then sharply raised above the atmospheric pressure. High temperature and pressure work in concert to create high-crystalline materials in a single step without the need for post-annealing procedures. When it is challenging to dissolve the precursors at room temperature or low temperatures, this method comes in handy. Growing nanoparticles is also beneficial if the material has a high vapor pressure close to its melting point.

Figure 3.1 Hydrothermal set-up

An autoclave is a sealed reactor used for the hydrothermal process. It is a robust vessel made to resist high pressure and temperature. Autoclaves are made up of cylindrical vessels with thick steel walls and hermetic sealing, which enables them to withstand high pressure and heat levels regularly for an extended period. Hydrothermal reactors are typically metal autoclaves lined with Teflon or an alloy to shield the autoclave body from the corrosive solvent.

3.1.1 Factors affecting the hydrothermal method

3.1.1.1 Temperature

Temperature has an important role in hydrothermal. It affects the solubility of precursors, nucleation, and crystal growth. While the reaction is happening at higher temperatures, which favors the increase in solubility of materials in the solvent, extremely high temperature leads to particle agglomeration or unwanted phase formations. So, the choice of temperature is very crucial in this method, as it decides whether the growth is kinetic or thermodynamic. A moderate temperature is required for the formation of metastable phases. Temperature also affects size, shape, and degree of crystallinity [27]. Depending on the material under consideration, hydrothermal reactions typically occur within a specific temperature range of 100°C to 300°C.

3.1.1.2 Pressure

Pressure plays a vital role in hydrothermal. The pressure is not externally added to the container but created naturally inside the sealed container, called an autoclave. When water or any other solvent is heated above its boiling point in a closed system, the steam cannot escape from there, it creates an internal pressure called autogenous pressure. While doing this, it helps the substances to dissolve in the solvent which are not dissolve at normal room temperature, for example, some high-density crystals only form under these conditions. At higher pressure, the atoms or ions can easily move through the solution and stick together with the growing crystal. So, maintaining proper pressure in hydrothermal will make sure that the particles have better quality, size control.

3.1.1.3 Time

Time decides how long the chemical reaction should be carried out in the autoclave. When we heat the material, it will start dissolving in the solution, and as longer we keep the crystals, the more it will grow and become more perfect. The reaction time is too much less it leads to an incomplete reaction. If the reaction takes a longer duration, it leads to problems like particles becoming a larger size, agglomeration, and ostward ripening, resulting in a product with uneven size. So, finding the right balance in time is very important. The time required depends on the material we are using, its size, shape, and how perfectly the crystals are needed. By controlling time, we can make materials with high-quality and uniform nanomaterials.

3.1.1.4 pH of the solution

pH of the solution is very crucial because it controls how the material dissolves and grows. pH tells us about whether the solution is acidic (less than 7 pH), neutral (pH 7), or basic (more than 7 pH). In acidic solutions, the materials dissolve better, and the reaction happens more slowly and carefully. This leads to the formation of smaller and well-shaped crystals. Acidic conditions are good for synthesizing certain oxides and other materials. In basic solutions s the reaction happens faster, so the materials growth also faster and crystals are formed in different shapes, like rods, wires, etc. So, pH controls the hydrolysis reaction. Therefore, by carefully adjusting pH for our requirements, we can make perfectly sized and quality particles. Song Q et al. reported that by maintaining a pH of 2.5 to 6.4, the particle (LFP) gets an orthorhombic structure [28].

3.1.1.5 Type and concentration of precursors

Precursors are more important like other parameters because it the starting material for hydrothermal processing. The type and concentration decide how the reaction happens, how fast the reaction happens, what the final product is, etc. Different types of precursors dissolve differently in water, react at different speeds, and form different crystal structures. The concentration of precursors depends on how much of it we are adding to the solution. If the concentration is low, the reaction happens slowly, and we do not get enough product. When

the concentration is too much more the solution becomes more crowded, as a result, the particles formed become clumpy or of uneven sizes. So, we should be careful about the concentration and type of precursors.

3.2 Materials used

Iron(II) sulphate ($FeSO_4 \cdot 7H_2O$), phosphoric acid (H_3PO_4), lithium hydroxide (LiOH), sugar ($C_6H_{12}O_6$), multi-walled carbon nanotube (MWCNT), polyvinylidene fluoride (PVDF), N-methyl-2-pyrrolidone (NMP), potassium hydroxide pellets (KOH), sodium hydroxide pellets (NaOH). These are materials used for the synthesis of LFP/MWCNT composite. The chemicals were used directly, without going through any further purification.

3.3 Synthesis of $LiFePO_4$

The process starts with measuring all precursors by using a weighing machine. We made a solution of lithium hydroxide (LiOH), phosphoric acid (H_3PO_4), and Iron(II) sulfate ($FeSO_4 \cdot 7H_2O$) which taken in molar ratio 3:1:1. Taken 0.768g/L of phosphoric acid (H_3PO_4), put 22g/L of Iron(II) sulfate ($FeSO_4 \cdot 7H_2O$) and sugar used as reducing agent. Do magnetic stirring for 30 minutes, then after the 30 minutes, add 0.569g/L of lithium hydroxide (LiOH). Stir the entire solution for 5 hours and 30 minutes using a magnetic stirrer. After a total of 6 hours of stirring, take the solution in a cleaned, sealed container (autoclave) and keep it at a temperature of 200℃ in a hot air oven for 10 hours. After the hydrothermal process, switch off the oven and, after cooling, take the solution and filter off the solution using a filter paper (11µm pore size). Make the remains dry at 80℃ in a hot air oven for 2 hours. After the time, take the powder from the dried filter paper and grind the powder very well with the mortar and pestle. Then, finally, we get the fine powder of $LiFePO_4$.

$$3LiOH + FeSO_4 + H_3PO_4 \xrightarrow{\text{sugar}} LiFePO_4 + Li_2SO_4 + H_2O$$

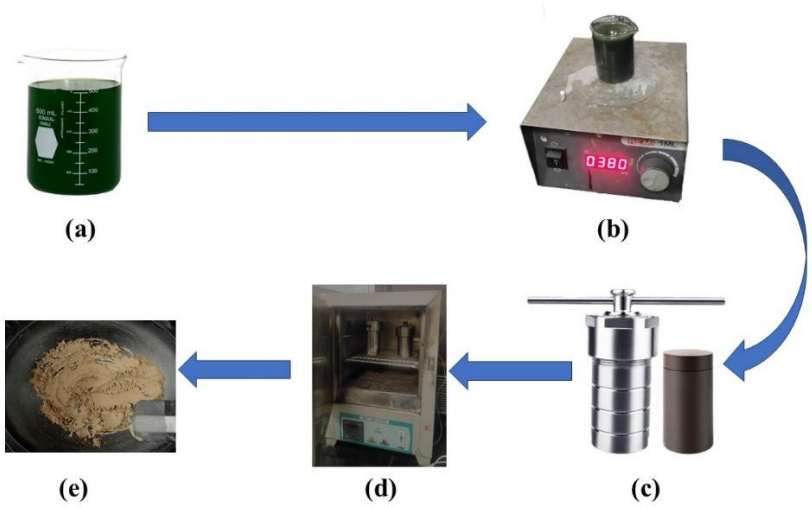

Figure 3.2 (a) solution, (b) Magnetic stirring for 6 hrs., (c) Solution put in autoclave, (d) Hydrothermal set up, (e) Powder of LFP after grinding

3.4 Electrode preparation

Ni foam (NF) is used as the current collector in the electrode preparation process. It is surface-treated by first washing it with 2M HCl and then ultrasonically treating it for 15 minutes. Deionized water and then acetone were used to repeat the same procedure. This process removes the oxide layer from the Ni foam's surface, and it was dried at 80 ℃ in a vacuum oven to prevent additional oxidation. We are making an electrode of LFP/MWCNT in the weight ratio of 1:0.3. Measure 0.080g of active material, 0.019g of multi-walled carbon nanotube (MWCNT), and 0.050g of polyvinylidene fluoride (PVDF). Put all three in 50ml beaker, add 30 mL of N-methyl-2-Pyrrolidone (NMP) solvent make a slurry. After creating a slurry, it was ultrasonically treated for 6 hours. PVDF's function is to serve as a binder. The final step involved creating the electrode using the dip and dry method, which involved applying the prepared slurry to the Ni foam surface and drying it for eight hours at 80 degrees Celsius in a hot air oven. The initial drying is done with the help of infrared light shown in Figure 3.3. Electrochemical analyses of the prepared LFP/MWCNT electrode revealed the electrode's electrochemical performance.

Figure 3.3: Initial drying process of deposited electrode

3.5 Characterization techniques

The material's physical and chemical characteristics were investigated using a variety of characterization techniques. A study of characteristics like structure, surface morphology, electrical, thermal, mechanical, optical, etc., is necessary for understanding the chemistry and 2physics of materials. In this work, we have investigated the surface morphology and structural properties of the generated $LiFePO_4$ and $LiFePO_4$/MWCNT composite using Raman spectroscopy, SEM, and XRD. The specific capacitance of the electrode is determined by electrochemical characterization methods such as GCD and CV.

3.5.1 Structural characterization

3.5.1.1 X-ray Diffraction (XRD)

X-ray diffraction is widely used to analyze crystal structures and atomic spacing. X-ray diffraction results from constructive interference between monochromatic X-rays and a crystalline sample. An electron beam generator known as a cathode ray tube directs concentrated, collimated X-rays at the sample. The incident ray interacts with the sample if

Bragg's condition is met, producing constructive interference (along with a wavelength that is diffracted).

$$n\lambda = 2dsin\theta \tag{3.1}$$

where d is the interplanar distance, θ is the diffraction angle, n is an integer, and λ is the wavelength of the x-ray used.

This law connects the diffraction angle, crystal lattice spacing, and electromagnetic radiation wavelength. After that, we identify, assess, and tally these diffracted X-rays. The powdered material's random arrangement allows for sample scanning through a range of 2θ angles to obtain potential lattice diffraction in all directions. Since each compound has a unique set of d-spacings, the diffraction peaks can be converted to d-spacing values to identify the compound. This is typically accomplished by comparing d-spacings to standard reference patterns [29]. The D8 Quest system Bruker diffractometer is used for XRD analysis. And the crystalline size is calculated by the Debye-Scherrer equation

$$\mathrm{L} = \frac{K\lambda}{\beta cos\theta} \tag{3.2}$$

Where L is the crystalline size, K is the Scherrer constant, $\boldsymbol{\lambda}$ is the wavelength of the X- ray, β is the full width half maxima, and θ is the Bragg's angle

3.5.1.2 Scanning Electron Microscopy (SEM)

Scanning electron microscopy (JEOL Model JSM-7600F) is used in many academic fields worldwide. It is considered an effective method for analyzing both organic and inorganic materials on the nanoscale to the micrometer (μm) scale. For a wide range of materials, SEM can create extraordinarily accurate images at high magnifications of up to 300,000x and even 1000000 (in some modern versions). The analysis will be performed using a high-energy electron beam with an electron voltage ranging from 100 to 30,000 volts.

A heat source is frequently used to achieve electron emission. Because the spot size created by the cannon is too big to create a sharp image, the SEM has lenses that compress the spot and concentrate the electrons on the specimen. Because electrons obtained from the final lens interact with the material and penetrate to a depth of 1μm, the majority of SEMs

have a spot size of less than 10 nm. These signals are then used to create an image. The movement of the scan coils creates the image of the specimen point by point, guiding the electron beam to certain locations in the form of straight lines until a rectangular raster is produced on the specimen's surface.

An electron detector looks for signals that cause the material being scanned to release electrons. Secondary electrons (SE) and backscattered electrons (BSE) are the two types of electrons that are used to produce SEM images. Both SE and BSE will be collected when a positive voltage is applied to the collector screen. But only when a negative voltage is applied to the collector screen will it collect BSE. Once the signals appear on the viewing screen, the operator adjusts brightness and intensity to create a reasonably clear image [30].

3.5.1.3 Raman spectroscopy

To learn about molecular vibrations, which can reveal information about a molecule's structure, symmetry, electrical environment, and bonding, Raman spectroscopy uses scattered light. This data makes it possible to analyze specific molecules both quantitatively and qualitatively. The two results of exposing a molecule to monochromatic light are elastic and inelastic light scattering. Inelastic scattering does not alter the photon's energy, wavelength, or frequency. A shift in photon frequency caused by the activation or deactivation of molecular vibrations is known as inelastic scattering, and it can result in a photon gaining or losing energy. As a result, three types of phenomena are possible.

At first, a molecule may interact with light, but no net energy exchange (E) occurs. The dispersed light's frequency is therefore equal to the incident light's ($E=E_o$). This process is known as Rayleigh scattering. Second, light can interact with a molecule to exchange energy equivalent to one molecular vibration. When a light photon receives vibrational energy from the molecule due to the contact, anti-Stokes Raman scattering takes place. In this instance, the scattered light's frequency ($E = E_o + E_v$) is higher than the incident light's frequency. Finally, if the contact causes the molecule to gain energy from the photon and the frequency of the scattered light is lower than that of the incident light ($E = E_o - E_v$), the process is known as Stokes Raman scattering.

A Raman spectrometer consists of a light source, detector, sample holder, and monochromator. A stable instrumentation, a high signal-to-noise ratio, and sufficient resolution are a few factors that can affect the analysis of Raman spectra. The two primary technologies used to collect the Raman spectra are dispersive Raman spectroscopy and Fourier transform Raman spectroscopy, which differ in their laser sources and techniques for identifying and analyzing Raman scattering[31]. It was done using the NOST HEDA-URSM 4/5/7 system for Raman spectroscopy.

3.5.1.4 Energy -Dispersive X-ray Spectroscopy (EDS)

EDS makes use of the X-ray spectrum that is created when a solid sample is exposed to a strong electron beam to obtain a localized chemical analysis. All elements from atomic number 4 (Be) to 92 (U) can theoretically be identified, though not all equipment can detect "light" elements ($Z < 10$). Because X-ray spectra are so straightforward, qualitative analysis only needs to identify the lines in the spectrum. To ascertain the concentrations of the elements present, quantitative analysis measures the line intensities for each element in the sample and for the same elements in calibration standards of available composition.

To create element distribution images, or "maps," the beam is scanned in a raster pattern similar to that of a television, and the intensity of a selected X-ray line is displayed. The images produced by the extracted electrons from the material can also show variations in mean atomic number or surface topography, depending on the mode selected. Similar to the electron probe, the scanning electron microscope (SEM) is typically used to produce electron images, but with the addition of an X-ray spectrometer, it can also be used for element mapping and even point analysis. As a result, these instruments' goals substantially overlap.

3.5.2 Electrochemical characterization

To maintain the electrochemical stability of the sensor, an electrical device called a potentiostat transforms the sensor's output into an analogue signal. The device consists of three electrodes immersed in an electrolyte: a reference electrode that keeps the electrolyte at a predetermined potential, a counter electrode, and the working electrode, which is where the

appropriate reaction (oxidation/reduction) takes place and to which biomolecular probes can be attached. Usually, silver or silver chloride is utilized as the reference electrode, and a platinum wire serves as the counter electrode. Conventional calomel electrodes are also frequently employed. The working electrode can be made of several materials, including carbon, platinum, gold, silver, and mercury. Because the reference electrode absorbs a constant voltage, current cannot flow through it. The potential of the working electrode is measured concerning it. A reference electrode's primary function is to act as a reference for measuring and managing the working electrode's potential; no current is ever passed through it. On the other hand, the counter electrode permits the entire current required to balance the current observed at the working electrode. Supercapacitors are commonly electrochemically characterized using cyclic voltammetry (CV) and galvanostatic charge-discharge (GCD.

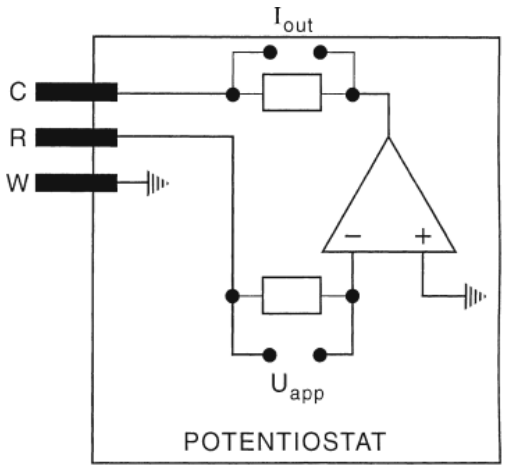

Figure 3.4: Schematic circuit diagram for a three-electrode potentiostat system

3.5.2.1 Cyclic Voltammetry (CV)

Cyclic voltage monitoring, or CV, is a technique used to identify the developing current in an electrochemical cell when the cell's voltage exceeds what the Nernst equation predicts. The process of CV involves measuring the current that flows out of a functional electrode potential on a regular basis. An applied potential is produced, which produces an excitation signal, when the potential of the working electrode is compared to a reference electrode that keeps its potential constant.

A negative, forward scan is the first thing the prospective does, beginning with a higher potential and ending with a lower potential. The potential extrema, sometimes referred to as the switching potential, is the point at which the analyte's voltage is sufficiently high to cause an oxidation or reduction. The potential performs well on the reversal scan. It should be mentioned that some analytes oxidize before other reactions take place, in which case, the potential would initially scan favorably. The scan rate can be changed to repeat this cycle. The scan rate is determined by the slope of the excitation signal. The current at the working electrode is measured during the potential scans to produce a cyclic voltammogram [32].

3.5.2.2 Galvanostatic Charge Discharge (GCD)

When a steady current density is applied and the potential towards time curve is plotted, the SC is evaluated using an equation in GCD studies.

$$C = I\ \Delta t\ /m\ \Delta V \tag{3.3}$$

where I is the current, V is the potential range, Δt is the discharge duration, and m is the mass of the active material. It is important to choose the discharge time and current density parameters so that the SC undergoes the most charge-discharge cycles without noticeably decreasing. In contrast, the SC typically decreases as the number of cycles increases. The number of charge-discharge cycles that can be obtained for galvanostatic tests depends on the amount of current needed [33].

CHAPTER 4: RESULTS AND DISCUSSIONS

4.1 Structural characterization

4.1.1 X-ray Diffraction (XRD)

The phase and crystallographic structure of the prepared LFP and LFP/MWCNT composite were investigated using X-ray powder diffraction (XRD). The prepared sample's well-defined diffraction pattern, shown in Figure 4.1, provides information about the excellent crystalline nature of LFP. The planes (200), (101), (111), (211), (301), (311), and (222) are represented by the high-intensity peaks that are obtained at 2θ values 17.14°, 20.74°, 25.58°, 29.82°, 32.18°, 35.60°, and 52.52°, respectively. The planes (210), (121), (410), (102), (112), (022), (131), (412), (610), (331), and (013) are indicated by the remaining, less intense peaks reached at 22.74°, 36.62°, 37.94°, 39.76°, 42.2°, 49.22°, 50.36°, 54.98°, 55.46°, 56.64°, and 62.06°, respectively. Based on the JCPDS card number 01-083-2029, the generated XRD data provides an idea of the olivine structure of LiFePO4. It was determined that the crystal's lattice parameters were a=10.334 A°, b=6.01 A°, and c=4.693 A°. Using the Debye-Scherrer equation, we determined the crystalline structure and obtained 50.75 nm.

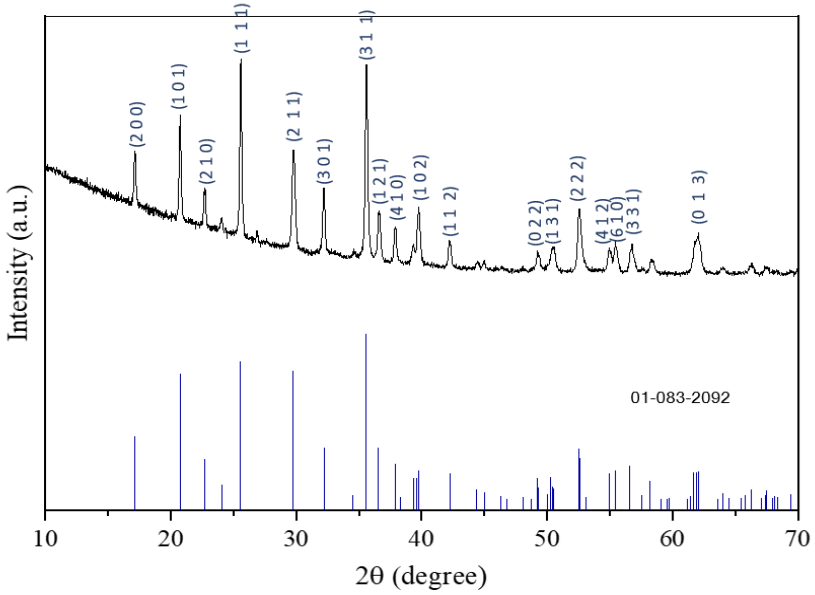

Figure 4.1 Diffraction pattern of $LiFePO_4$

After that, we took the XRD of the LFP/MWCNT composite. Figure 4.2 shows the diffraction pattern of LFP and MWCNT. We can see that there are some more peaks compared to the XRD of LFP. From Figure 4.3, we can see that the characteristic peaks of carbon come at 26.88^{o} and 43.8^{o}, corresponding to the planes (002) and (101), respectively. The actual values are 26.5^{o} and 44^{o}, corresponding to the planes (002) and (101). It matches our experimental values; from this, we can conclude that the MWCNT is successfully blended with LFP [34]

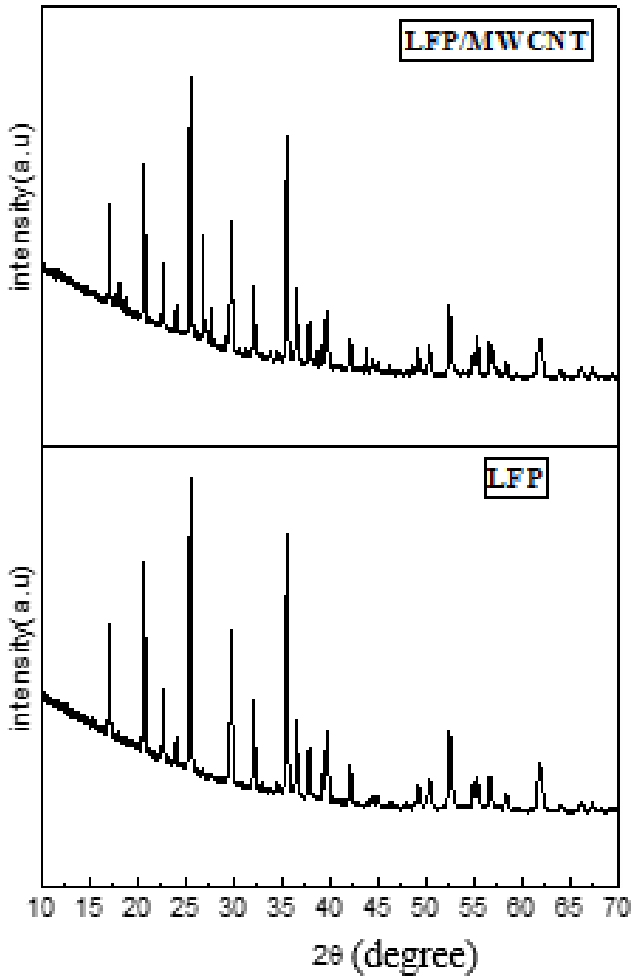

Figure 4.2 Diffraction pattern of $LiFePO_4$ and LiFePO4/MWCNT composite

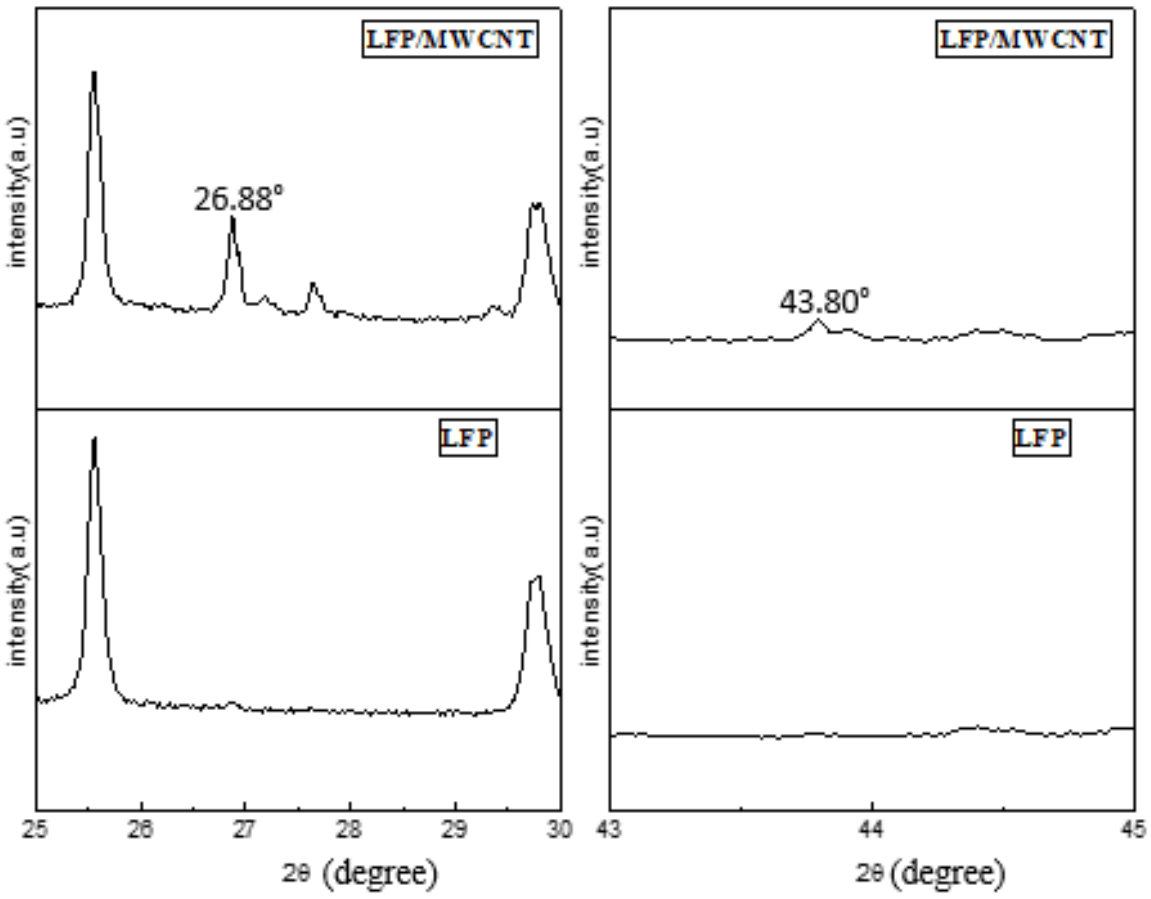

Figure 4.3 Comparison between the diffraction peaks of LiFePO4 and LiFePO4/MWCNT composite

4.1.2 Scanning Electron Microscopy (SEM)

The SEM images of LFP are shown in Figure 4.4. From this, we are getting a better picture of $LiFePO_4$ It is found to be rectangular and pebble-shaped, suggesting a uniform, stable morphology, which is beneficial for structural integrity and long cycle life. The surfaces are rough and textured, with some showing agglomerates. Voids and cracks are seen very little, so a dense packing can be observed from the images.

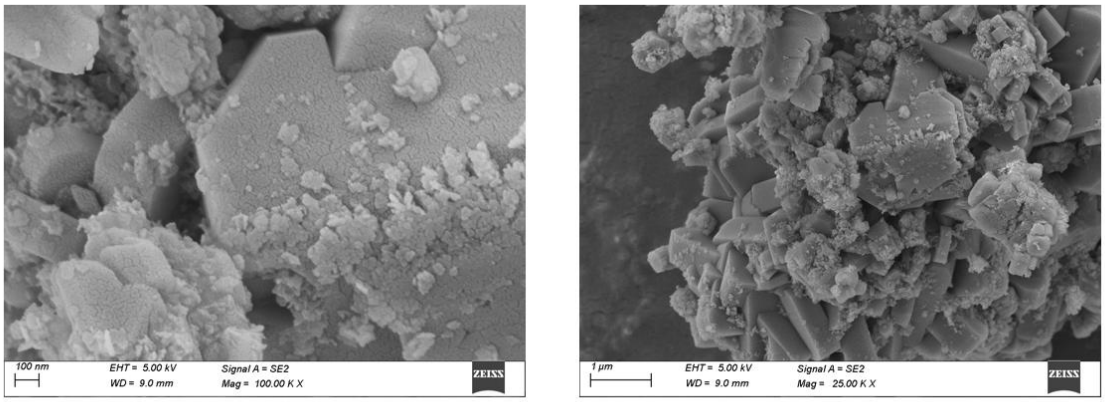

(a) (b)

Figure 4.4 SEM images of $LiFePO_4$

The SEM images of LFP/MWCNT are shown in Figure 4.5. From the images, we can see that the fibrous or tubular structures can be seen above the rectangular pebble-shaped LFP. This tubular appearance is the characteristic structure of multi-walled carbon nanotubes. In order to reduce inter-particle resistance and speed up electron transfer during supercapacitor charge and discharge, the MWCNTs create a bridge between the LFP particles. Furthermore, this network aids in preserving structural integrity, particularly during the frequent volume changes that take place during cycling.

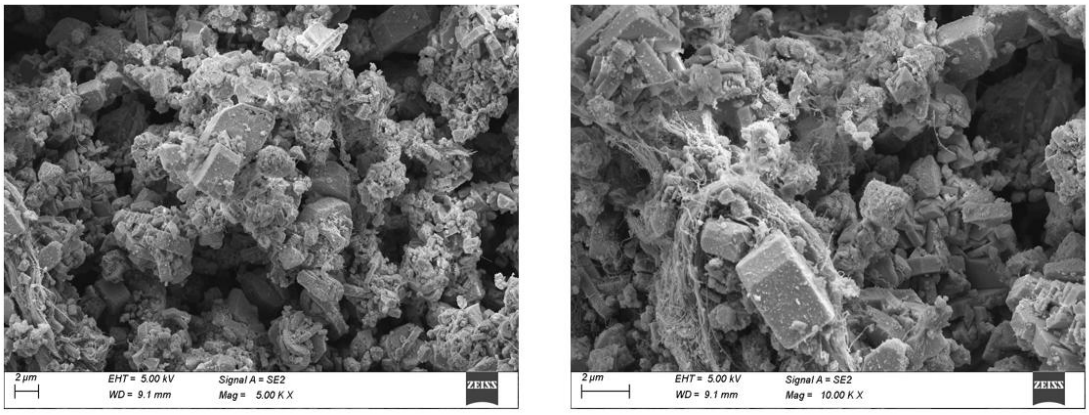

(c) (d)

Figure 4.5 SEM images of $LiFePO_4$/MWCNT

4.1.3 Raman Spectroscopy

The Raman spectrum of $LiFePO_4$ is shown in Figure 4.6. The presence of the Raman shift is shown from 163 cm^{-1}. The information about the symmetric stretching mode of PO_4 (P-O bond stretching) is given by the peak at 996 cm^{-1}, the symmetric bending mode of PO_4 (O-P-O bond) is obtained at the shift of 564 cm^{-1}, asymmetric bending of PO_4 gets a shift of 621 cm^{-1}, the coupled translation and vibrational motion of Fe and PO_4^{3-} giving the shift of 163 cm^{-1}, 214 cm^{-1}, and 217 cm^{-1}, asymmetric stretching of the PO_4 unit giving shift 1048 cm^{-1}, and 1162 cm^{-1}, Fe-O stretching vibration is given by 310 cm^{-1}. All the values are matching with the standard characteristic shift of our active material [35].

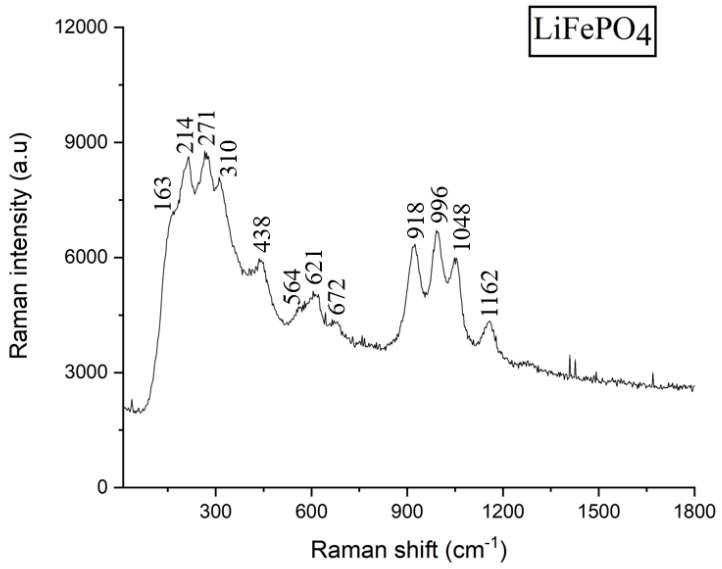

Figure 4.6 Raman spectrum of $LiFePO_4$

Next, we took the Raman spectrum of our composite material $LiFePO_4$/MWCNT, shown in Figure 4.7. By analyzing the graph, we are getting the values of the D band and the G band of carbon are 1332.89 cm^{-1} and 1571.61 cm^{-1}. It is coming in the characteristic range of the D band (1300 to 1400 cm^{-1}) and G band (1580 cm^{-1}) [36].

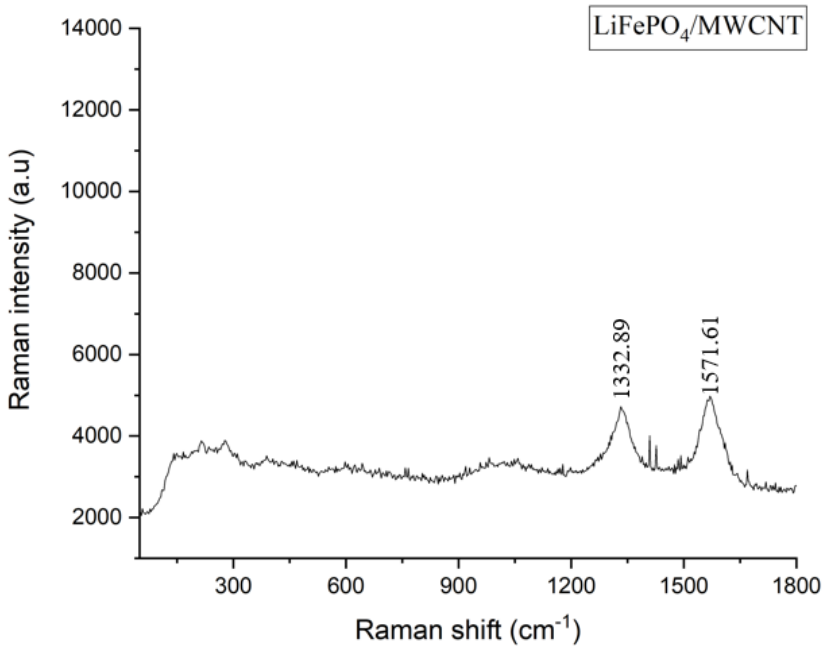

Figure 4.7 Raman spectrum of $LiFePO_4$/MWCNT

4.1.4 Energy-Dispersive X-ray Spectroscopy (EDS)

The analysis of the elements in the prepared $LiFePO_4$ is performed by EDS. Figure 4.8 depicts the results. The atomic weights of O, P, and Fe are obtained as 62.62%, 14.44%, and 22.94%, respectively. The elemental mapping gives the idea that the elements O, P, and Fe are distributed uniformly in the material.

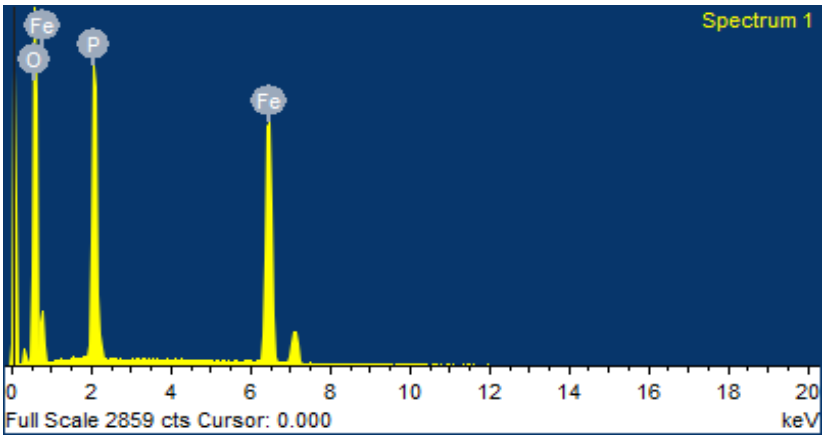

Figure 4.8 EDS Spectrum of $LiFePO_4$

Element	Atomic weight %	Weight%
O	62.62	36.70
P	14.44	16.38
Fe	22.94	46.93

Table 4.1 Atomic weight% % and weight% of elements in $LiFePO_4$

The analysis of the elements in the prepared $LiFePO_4$/MWCNT is performed by EDS. Figure 4.9 depicts the results. The atomic weights of C, O, P, and Fe are obtained as 34.33%, 45.74%, 7.83%, and 12.09%, respectively. The elemental mapping gives the idea that the elements C, O, P, and Fe are distributed uniformly in the material.

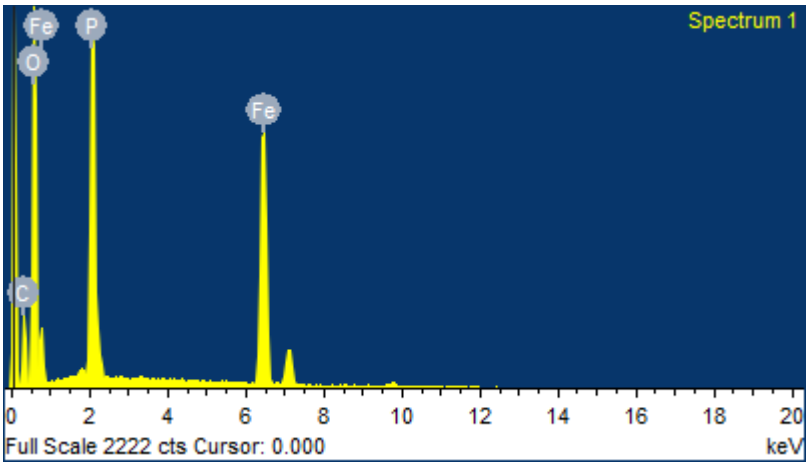

Figure 4.9 EDS Spectrum of $LiFePO_4$/MWCNT

Element	Atomic weight %	Weight%
C	34.33	20.00
O	45.74	35.49
P	7.83	11.77
Fe	32.75	12.09

Table 4.2 Atomic weight% % and weight% of elements in LiFePO4/MWCNT

4.2 Electrochemical Characterization

This method uses platinum (Pt) wire as the counter electrode, $LiFePO_4$/MWCNT as the working electrode, and Hg/HgO as the reference electrode. The potential window range was kept between 0 and 0.7 V v/s Hg/HgO.

4.2.1 Cyclic Voltammetry (CV)

The electrochemical behavior of the generated $LiFePO_4$/MWCNT electrode, with Hg/HgO serving as the reference electrode, was investigated using cyclic voltammetry over a voltage range of 0 V to 0.7 V v/s Hg/HgO at various scan rates in 3M LiOH solution. The capacitance properties were primarily caused by faradaic redox processes, as demonstrated by the CV (Figure 4.10) curve, which showed clear and distinct redox peaks.

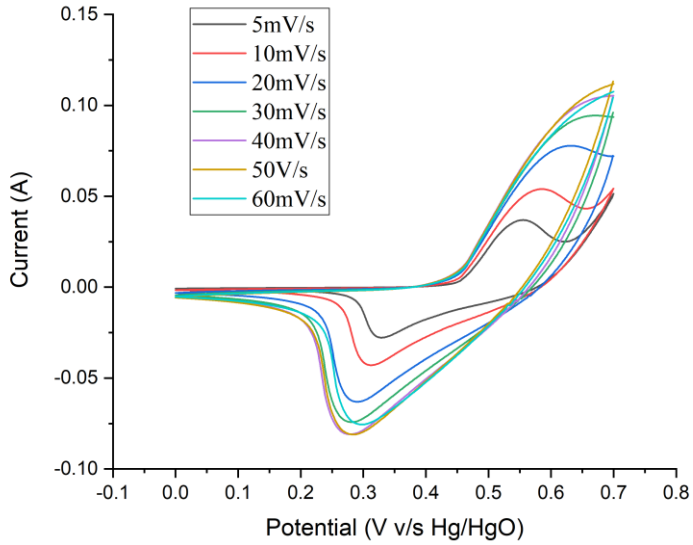

Figure 4.10 CV curve of LiOH with different scan rates

The specific capacitance of the electrode is evaluated by using the equation,

$$C_s = \frac{\int iVdV}{\vartheta w \Delta V}(F/Kg) \tag{4.1}$$

where, $\int iVdV$ indicates the area under the CV curve, ϑ gives the scan rate, w is the mass of material deposited on the electrode, and ΔV It is the potential window.

Sl No.	Scan rate (mV/s)	Specific capacitance (F/kg) $\times 10^4$
1	5	86.65
2	10	73.12
3	20	56.80
4	30	43.24
5	40	35.05
6	50	26.89
7	60	21.33

Table 4.3 Specific capacitance of LiOH in different scan rates

From Table 4.3, we are getting the highest specific capacitance of 86.65×10^4 F/kg at 5mV/s. So, we kept the scan rate as 5mV/s and performed cyclic voltammetry in 3M NaOH and 3M KOH electrolytes. The CV plots are depicted in Figure 4.11

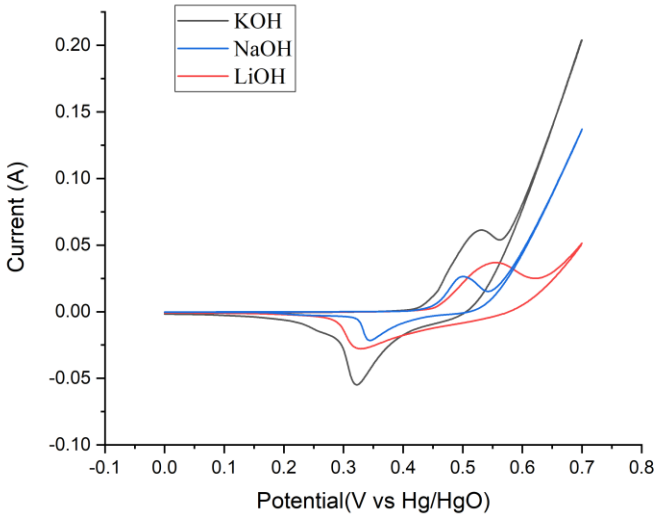

Figure 4.11 CV curve in different electrolytes with a scan rate of 5mV/s

Sl No.	Electrolyte	Specific capacitance (F/kg) $\times 10^4$
1	LiOH	86.65
2	NaOH	38.89
3	KOH	108.09

Table 4.4 Specific capacitance of different electrolytes with a scan rate of 5mV/s

From Table 4.4, we can conclude that the highest specific capacitance of 108.09×10^4 F/kg is obtained in 3M KOH electrolyte at a scan rate of 5mV/s. The value of energy density we obtained is 73.56 Wh/Kg, and power density 1819.48 W/Kg

4.2.2 Galvanostatic Charge Discharge (GCD)

The LiFePO4/MWCNT electrode is subjected to GCD at various current densities. 0 to 0.7V vs Hg/HgO was the potential window setting. The findings in Figure 4.12. The following formula is used to determine the electrode's specific capacitance:

$$C_s = \frac{I \times (\Delta t)}{(\Delta V)} \tag{4.2}$$

$I, \Delta t$ and ΔV are the current density, discharging time, and potential window, respectively. The energy density (E) and power density (P) of the electrode material are calculated by the following equations,

$$E = \frac{C_s \times \Delta V^2 \times 10}{2\times36} \text{ (Wh/kg)} \tag{4.3}$$

$$P = \frac{E}{\Delta t} \text{ (W/kg)} \tag{4.4}$$

Table 4.5 provides the electrode's specific capacitance, energy density, and power density for various current densities. It indicates that a current density of 2 A/g yields the maximum

specific capacitance value of 965.40 F/g. The trend indicates that the specific capacitance for the supercapacitor electrode is decreasing as the current density increases.

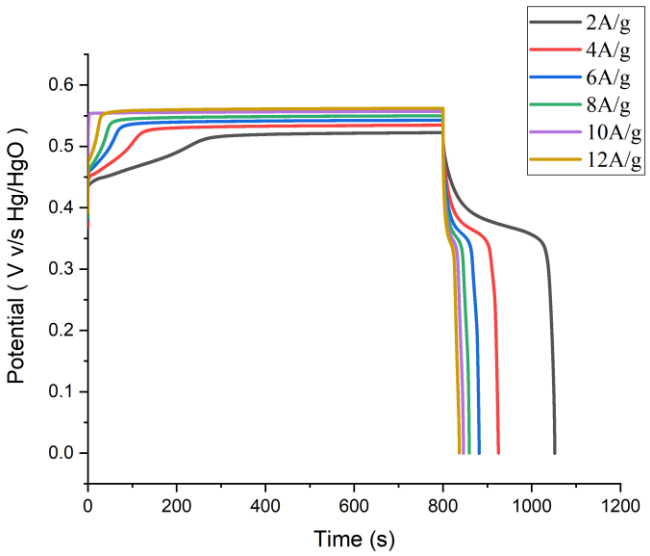

Figure 4.12 GCD profile at different current densities

Sl No.	Current density (A/g)	Specific capacitance (F/g)	Energy density (Wh/Kg)	Power density (W/Kg)
1	2	965.40	36.53	521.91
2	4	934.90	37.02	1067.79
3	6	904.87	36.91	1625.59
4	8	863.41	36.27	2199.66
5	10	830.70	35.79	2784.61
6	12	760.67	33.36	3243.20

Table 4.5 The specific capacitance, energy density, and Power density of the electrode for different current densities

4.2.3 Electrochemical Impedance Spectroscopy (EIS)

An electrochemical impedance spectroscopy (EIS) study was conducted in the frequency range of 0.1 Hz to 10^5 Hz to evaluate ion conduction and transfer mechanisms at open circuit potential. Figure 4.13 displays a Nyquist plot.

The Nyquist plot analysis yields a semicircle at the high frequency zone and a straight line at the low frequency zone. The solution resistance (R_s) value is found at the graph's intersection with the x-axis. The inherent resistance of the electrode material, the resistance arising from the 3M aqueous KOH electrolyte, and the interface resistance brought on by the contact between the active electrode material and the current collector are all included in the solution resistance.

The Nyquist plot indicates that the electrical conductivity is excellent, with the value of R_s being 0.661Ω.

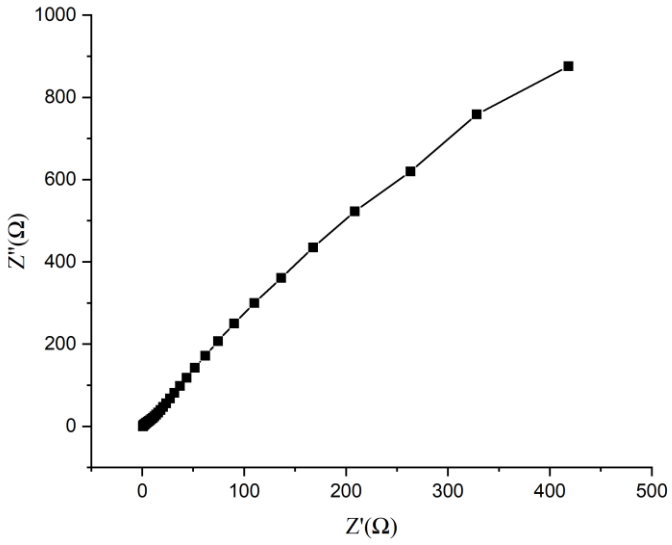

Figure 4.13 Nyquist plot of LFP/MWCNT

4.2.4 Cycling Stability

At a higher scan rate of 150 mV/s, the LFP/MWCNT electrode was exposed to 2000 continuous cyclic voltammetry cycles. This was carried out to evaluate the electrode's cyclic stability. The results demonstrate that the material hardly degrades during electrochemical operations at high scan rates, with a capacitance retention of 68.64% over 2000 cycles. Shown in Figure 4.14

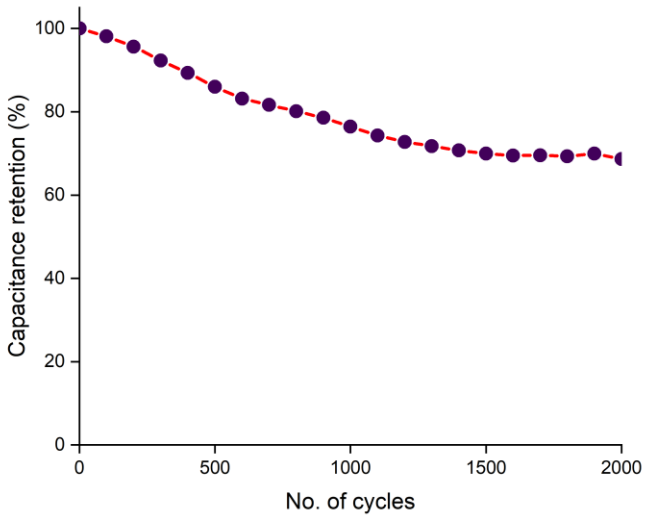

Figure 4.14 Cycling Stability of LFP/MWCNT electrode

CHAPTER 5: CONCLUSION

In the present study, the bottom-up method, hydrothermal synthesis, was used to fabricate two-dimensional lithium iron phosphate (LFP) with a crystallite size of 50.75 nm. Using MWCNT, a composite with a weight ratio of 1:0.3 was made. These composites were deposited on a three-dimensional Ni foam current collector to form an electrode. We tested the electrode in 3M solutions of LiOH, NaOH, and KOH. In 3M KOH, we got better results. The resulting electrode had an impressive specific capacitance of 965.40 F/g under 2 A/g current density. The GCD data showed a greater power density of 521.91 W/kg and a higher energy density of 36.53 Wh/kg at a current density of 2 A/g. Importantly, the non-linear shape of the GCD curves and the peak shape of the CV curves suggest that the materials as manufactured are exhibiting properties more likely to be those of a battery-type electrode. The findings highlight the efficient application of lithium iron phosphate as a possible electrode for energy storage devices exhibiting strong performance.

REFERENCES

[1] W. Raza *et al.*, “Recent advancements in supercapacitor technology,” Oct. 01, 2018, *Elsevier Ltd*. doi: 10.1016/j.nanoen.2018.08.013.

[2] A. A. Kulkarni, V. A. Savekar, T. S. Bhat, and P. S. Patil, “Recent advances in metal pyrophosphates for electrochemical supercapacitors: A review,” Aug. 15, 2022, *Elsevier Ltd*. doi: 10.1016/j.est.2022.104986.

[3] N. L. Panwar, S. C. Kaushik, and S. Kothari, “Role of renewable energy sources in environmental protection: A review,” Apr. 2011. doi: 10.1016/j.rser.2010.11.037.

[4] A. A. Mirghni, K. O. Oyedotun, B. A. Mahmoud, A. Bello, S. C. Ray, and N. Manyala, “Nickel-cobalt phosphate/graphene foam as enhanced electrode for hybrid supercapacitor,” *Compos B Eng*, vol. 174, Oct. 2019, doi: 10.1016/j.compositesb.2019.106953.

[5] S. Nivetha, S. Prabahar, R. T. Karunakaran, M. Narendhera Ganth, and S. Dhinesh, “Effect of Fe dopant concentration on electrochemical properties of Ni2P2O7 thin films,” *Inorg Chem Commun*, vol. 146, Dec. 2022, doi: 10.1016/j.inoche.2022.110193.

[6] M. Li *et al.*, “Facile Synthesis of Bimetal Nickel Cobalt Phosphate Nanostructures for High-Performance Hybrid Supercapacitors,” *J Alloys Compd*, vol. 893, Feb. 2022, doi: 10.1016/j.jallcom.2021.162340.

[7] Z. S. Iro, C. Subramani, and S. S. Dash, “A brief review on electrode materials for supercapacitor,” 2016, *Electrochemical Science Group*. doi: 10.20964/2016.12.50.

[8] N. I. Jalal, R. I. Ibrahim, and M. K. Oudah, “A review on Supercapacitors: Types and components,” in *Journal of Physics: Conference Series*, IOP Publishing Ltd, Aug. 2021. doi: 10.1088/1742-6596/1973/1/012015.

[9] A. A. Kulkarni, N. K. Gaikwad, A. P. Salunkhe, R. M. Dahotre, and T. S. Bhat, “Transition metal phosphates: A paradigm for electrochemical supercapacitors,” Nov. 01, 2023, *Elsevier B.V.* doi: 10.1016/j.jelechem.2023.117795.

[10] P. Forouzandeh, V. Kumaravel, and S. C. Pillai, “Electrode materials for supercapacitors: A review of recent advances,” Sep. 01, 2020, *MDPI*. doi: 10.3390/catal10090969.

[11] Q. Zong, C. Liu, H. Yang, Q. Zhang, and G. Cao, “Tailoring nanostructured transition metal phosphides for high-performance hybrid supercapacitors,” Jun. 01, 2021, *Elsevier B.V.* doi: 10.1016/j.nantod.2021.101201.

[12] M. M. Mezgebe *et al.*, “3D graphene-Fe3O4-polyaniline, a novel ternary composite for supercapacitor electrodes with improved electrochemical properties,” *Mater Today Energy*, vol. 5, pp. 164–172, Sep. 2017, doi: 10.1016/j.mtener.2017.06.007.

[13] F. Usman *et al.*, “Synthesis and characterisation of a ternary composite of polyaniline, reduced graphene-oxide and chitosan with reduced optical band gap and stable aqueous dispersibility,” *Results Phys*, vol. 15, Dec. 2019, doi: 10.1016/j.rinp.2019.102690.

[14] T. Das and B. Verma, “Polyaniline based ternary composite with enhanced electrochemical properties and its use as supercapacitor electrodes,” *J Energy Storage*, vol. 26, Dec. 2019, doi: 10.1016/j.est.2019.100975.

[15] S. Rudra, H. W. Seo, S. Sarker, and D. M. Kim, “Supercapatteries as Hybrid Electrochemical Energy Storage Devices: Current Status and Future Prospects,” Jan. 01, 2024, *Multidisciplinary Digital Publishing Institute (MDPI)*. doi: 10.3390/molecules29010243.

[16] A. G. Olabi, Q. Abbas, A. Al Makky, and M. A. Abdelkareem, “Supercapacitors as next generation energy storage devices: Properties and applications,” *Energy*, vol. 248, Jun. 2022, doi: 10.1016/j.energy.2022.123617.

[17] A. Muzaffar, M. B. Ahamed, K. Deshmukh, and J. Thirumalai, “A review on recent advances in hybrid supercapacitors: Design, fabrication and applications,” Mar. 01, 2019, *Elsevier Ltd*. doi: 10.1016/j.rser.2018.10.026.

[18] D. Gao, Z. Luo, C. Liu, and S. Fan, “A survey of hybrid energy devices based on supercapacitors,” Aug. 01, 2023, *KeAi Publishing Communications Ltd.* doi: 10.1016/j.gee.2022.02.002.

[19] S. Mandal *et al.*, “Recent advancement and design in supercapacitor hybrid electrode materials: Bridging the gap between energy and power density,” Mar. 01, 2025, *Elsevier B.V.* doi: 10.1016/j.ceja.2024.100690.

[20] G. G. Amatucci, F. Badway, A. Du Pasquier, and T. Zheng, “An Asymmetric Hybrid Nonaqueous Energy Storage Cell,” *J Electrochem Soc*, vol. 148, no. 8, p. A930, 2001, doi: 10.1149/1.1383553.

[21] N. W. K. Wan, H. N. Lim, I. Ibrahim, N. M. Huang, C. Y. Foo, and Z. T. Jiang, “Electrochemical performance of aqueous hybrid supercapacitor based on LiFePO4/Si/graphene composite,” *Chemical Engineering Journal*, vol. 456, Jan. 2023, doi: 10.1016/j.cej.2022.141132.

[22] P. F. R. Ortega *et al.*, “LiFePO4/Mesoporous Carbon Hybrid Supercapacitor Based on LiTFSI/Imidazolium Ionic Liquid Electrolyte,” *Journal of Physical Chemistry C*, vol. 122, no. 3, pp. 1456–1465, Jan. 2018, doi: 10.1021/acs.jpcc.7b09869.

[23] M. Y. Ho, P. S. Khiew, D. Isa, T. K. Tan, W. S. Chiu, and C. H. Chia, “LiFePO4 - Activated carbon composite electrode as symmetrical electrochemical capacitor in mild aqueous electrolyte,” in *Applied Mechanics and Materials*, Trans Tech Publications Ltd, 2014, pp. 3–6. doi: 10.4028/www.scientific.net/AMM.627.3.

[24] D. Vernardou, “Recent Report on the Hydrothermal Growth of LiFePO4 as a Cathode Material,” *Coatings*, vol. 12, no. 10, Oct. 2022, doi: 10.3390/coatings12101543.

[25] J. Hu, W. Huang, L. Yang, and F. Pan, “Structure and performance of the LiFePO4cathode material: From the bulk to the surface,” Jul. 28, 2020, *Royal Society of Chemistry*. doi: 10.1039/d0nr03776a.

[26] Q. Jing, J. Zhang, Y. Liu, W. Zhang, Y. Chen, and C. Wang, “Direct Regeneration of Spent LiFePO4Cathode Material by a Green and Efficient One-Step Hydrothermal Method,” *ACS Sustain Chem Eng*, vol. 8, no. 48, pp. 17622–17628, Dec. 2020, doi: 10.1021/acssuschemeng.0c07166.

[27] O. Xiuqin, P. Lin, G. Haichen, W. Yichen, and L. Jianwei, “Temperature-dependent crystallinity and morphology of LiFePO4 prepared by hydrothermal synthesis,” *J Mater Chem*, vol. 22, no. 18, pp. 9064–9068, May 2012, doi: 10.1039/c2jm30191a.

[28] Q. Song, X. Ou, L. Wang, G. Liang, and Z. Wang, “Effect of pH value on particle morphology and electrochemical properties of LiFePO4 by hydrothermal method,” *Mater Res Bull*, vol. 46, no. 9, pp. 1398–1402, Sep. 2011, doi: 10.1016/j.materresbull.2011.05.015.

[29] A. A. Bunaciu, E. gabriela Udriştioiu, and H. Y. Aboul-Enein, “X-Ray Diffraction: Instrumentation and Applications,” Oct. 02, 2015, *Taylor and Francis Ltd.* doi: 10.1080/10408347.2014.949616.

[30] A. Mohammed and A. Abdullah, “Scanning Electron Microscopy (SEM): A Review.” [Online]. Available: https://www.researchgate.net/publication/330168803

[31] R. S. Das and Y. K. Agrawal, “Raman spectroscopy: Recent advancements, techniques and applications,” Nov. 2011. doi: 10.1016/j.vibspec.2011.08.003.

[32] F. Marken, A. Neudeck, and A. M. Bond, “Cyclic voltammetry,” in *Electroanalytical Methods: Guide to Experiments and Applications*, Springer Berlin Heidelberg, 2010, pp. 57–106. doi: 10.1007/978-3-642-02915-8_4.

[33] M. A. ’AZAM MOHD ABID *et al.*, “Cyclic Voltammetry and Galvanostatic Charge-Discharge Analyses of Polyaniline/Graphene Oxide Nanocomposite based Supercapacitor,” *Malaysian Journal on Composites Science and Manufacturing*, vol. 3, no. 1, pp. 14–26, Sep. 2020, doi: 10.37934/mjcsm.3.1.1426.

[34] B. Ilkiv *et al.*, “Electronic structure of hollow graphitic carbon nanoparticles fabricated from acetylene carbon black,” *Fullerenes Nanotubes and Carbon Nanostructures*, vol. 23, no. 5, pp. 449–454, 2015, doi: 10.1080/1536383X.2014.885957.

[35] J. Wu *et al.*, “In situ Raman spectroscopy of LiFePO4: Size and morphology dependence during charge and self-discharge,” *Nanotechnology*, vol. 24, no. 42, Oct. 2013, doi: 10.1088/0957-4484/24/42/424009.

[36] Z. Li, L. Deng, I. A. Kinloch, and R. J. Young, “Raman spectroscopy of carbon materials and their composites: Graphene, nanotubes and fibres,” Jun. 01, 2023, *Elsevier Ltd*. doi: 10.1016/j.pmatsci.2023.101089.